TU Delft

Delft University of Technology

A critical review of discontinuity plane extraction from 3D point cloud data of rock mass surfaces

Daghigh, Hamid; Tannant, Dwayne D.; Daghigh, Vahid; Lichti, Derek D.; Lindenbergh, Roderik

DOI
10.1016/j.cageo.2022.105241

Publication date
2022

Document Version
Final published version

Published in
Computers and Geosciences

Citation (APA)
Daghigh, H., Tannant, D. D., Daghigh, V., Lichti, D. D., & Lindenbergh, R. (2022). A critical review of discontinuity plane extraction from 3D point cloud data of rock mass surfaces. *Computers and Geosciences*, *169*, Article 105241. https://doi.org/10.1016/j.cageo.2022.105241

Important note
To cite this publication, please use the final published version (if applicable).
Please check the document version above.

Copyright
Other than for strictly personal use, it is not permitted to download, forward or distribute the text or part of it, without the consent of the author(s) and/or copyright holder(s), unless the work is under an open content license such as Creative Commons.

Takedown policy
Please contact us and provide details if you believe this document breaches copyrights.
We will remove access to the work immediately and investigate your claim.

This work is downloaded from Delft University of Technology.
For technical reasons the number of authors shown on this cover page is limited to a maximum of 10.

Green Open Access added to TU Delft Institutional Repository

'You share, we take care!' - Taverne project

https://www.openaccess.nl/en/you-share-we-take-care

Otherwise as indicated in the copyright section: the publisher is the copyright holder of this work and the author uses the Dutch legislation to make this work public.

Computers & Geosciences 169 (2022) 105241

Contents lists available at ScienceDirect

Computers and Geosciences

journal homepage: www.elsevier.com/locate/cageo

A critical review of discontinuity plane extraction from 3D point cloud data of rock mass surfaces

Hamid Daghigh [a,*], Dwayne D. Tannant [a], Vahid Daghigh [b], Derek D. Lichti [c], Roderik Lindenbergh [d]

[a] School of Engineering, The University of British Columbia, Kelowna, BC V1V 1V7, Canada
[b] Department of Aerospace Engineering, Mississippi State University, Starkville, MS, USA
[c] Department of Geomatics Engineering, The University of Calgary, Calgary, AB T2N 1N4, Canada
[d] Department of Geoscience and Remote Sensing, Delft University of Technology, Stevinweg 1, 2628 CN Delft, Netherlands

ARTICLE INFO

Keywords:
Discontinuity plane extraction
Rock mass
Point cloud segmentation
Remote sensing
LiDAR
Unsupervised learning

ABSTRACT

Field investigations of geometric discontinuity properties in rock masses are increasingly using three-dimensional point cloud data. These point clouds sample the rock mass surface and are typically acquired by photogrammetry or LiDAR. The automatic segmentation and extraction of planar surfaces from point cloud data have attracted significant attention among researchers. This paper reviews the capabilities, merits, and limitations of different segmentation methods for discontinuity plane surface extraction and the specific challenges of processing point cloud data collected from rock faces. The segmentation and orientation results of a series of studies on two point cloud datasets of rock mass surfaces are critically discussed. A new set of ground truth orientations for one point cloud and some challenges faced while labeling a ground truth discontinuity plane are presented. Some suggestions to establish reliable and reproducible ground truth orientation results are presented. Two popular open-source software tools (CloudCompare and Discontinuity Set Extractor) for planar surface extraction are reviewed, and their capabilities and shortcomings are discussed. Acquisition of high-quality point cloud data and sharing it on a public repository establishes a basis for researchers to implement their methodologies and meaningfully compare their results to advance the knowledge in the field. Finally, some recommendations for future research and development are summarized.

1. Introduction

Advances in airborne and terrestrial remote sensing techniques to generate bare-earth point clouds have revolutionized various geoscience fields in the last decade. Light detection and ranging (LiDAR) and photogrammetry techniques are among the most common methods in remote sensing. These techniques can provide high accuracy and high-resolution 3D data for ground surfaces and remove the drawbacks of traditional measurement and geological mapping practices, which results in substantial improvement in the data acquisition process. The 3D surface data acquired from geometric remote sensing techniques are extensively used in geology, geotechnical engineering, and mapping surveys. Their applications cover a vast spectrum of practices, including hazard identification and monitoring (Herrera et al., 2010; Jones and Hobbs, 2021), analysis of volcanic activities (Fornaciai et al., 2010), landslides (Colesanti and Wasowski, 2006; Jaboyedoff et al., 2012a), earthquakes (Rathje and Franke, 2016), identification of fault areas (Chen et al., 2015), mapping ground texture (Yan et al., 2015), and geospatial analysis of data (de Oliveira et al., 2021; Deibe et al., 2020; Kong et al., 2020; Smith and Holden, 2021).

Rock masses often exhibit complex geomechanical behavior because of the presence of discontinuities. These discontinuities can affect the strength, deformability, and permeability of a rock mass. Therefore, the reliable design of an engineered structure on or within a discontinuous rock mass is closely linked to accurately characterizing and identifying the discontinuities involved. The reliability of traditional manual measurements of discontinuity orientations with a compass along an in-situ scanline depends on the amount of data collected and the bias involved during sampling (Priest and Hudson, 1981). Manual measurements are impossible in inaccessible regions or high steep slopes where there is a threat to human safety. In addition, the data collected are affected by the experience and skill of the geologist or engineer (Lato et al., 2012; Vöge

* Corresponding author.
E-mail addresses: hdaghigh@yahoo.com, hamid.daghigh@ubc.ca (H. Daghigh).

https://doi.org/10.1016/j.cageo.2022.105241
Received 26 March 2021; Received in revised form 19 September 2022; Accepted 23 September 2022
Available online 5 October 2022
0098-3004/© 2022 Elsevier Ltd. All rights reserved.

et al., 2013). On the other hand, the use of remote sensing techniques in rock engineering provides the following benefits: (i) automating the sampling procedure with a rapid collection of data in a safe mode, (ii) the possibility of mapping rock faces, irrespective of height and slope, (iii) minimum disruption to on-going operating activities, (iv) development of a permanent archival record of the collected data, (v) increased quantity of data with good accuracy, and (vi) minimizing the user subjective and bias interpretation during the data acquisition process.

In rock engineering, a variety of methods have been presented to automatically identify the geometric properties of discontinuity planes using various mathematical modeling techniques and available software packages. However, the task of plane detection and extraction from point cloud data of rock mass structures comes with unique challenges due to the irregularity of the rock surface, compounded by factors such as weathering, vegetation cover, noise, biases, and data gaps (empty areas in point cloud data). Therefore, it is imperative to implement new algorithms and techniques to address these challenges to achieve efficient detection and extraction of discontinuities planes from the surface of rock faces (Abellán et al., 2014).

The recently published review paper (Battulwar et al., 2021) covers a wide range of topics, including joint sets detection, persistence, joint spacing, roughness, and block size using point clouds, digital elevation maps, or mesh models. Conversely, the current critical review paper exclusively focuses on discontinuity plane extraction from 3D point cloud data. It brings breadth and depth by comprehensively reviewing methods and techniques and analyzing the discussion and results in the literature with a critical lens. Discussion regarding calculating more efficient discontinuity orientation practices for reliable comparison and verification is also presented.

Section 2 discusses the most common point cloud acquisition method, their characteristics, merits, and drawbacks in this critical review paper. Section 3 introduces and reviews various techniques to segment and extract planar surfaces and their geometric features from rock surface point cloud data. The challenges and limitations associated with these methods are summarized. Some recommendations to overcome these limitations are also presented. Section 4 critically discusses the qualitative and quantitative results of hybrid techniques implemented on rock face point clouds. The qualitative results explore the segmentation metrics and orientation on the plane surface of rock faces using two case studies. The advantages and disadvantages of the discussed methods are summarized. Some guidelines for generating reliable and reproducible ground truth orientations are also presented. Useful software tools for working with point cloud data are introduced, and two common open-access tools for processing point cloud data of rock masses are described in Section 5. Finally, Section 6 presents conclusions and recommendations and a summary of directions for future research.

2. 3D point clouds

A point cloud is a collection of points in 3D space representing the surface exposure of an object. Each point has a 3D coordinate (x, y, and z). In addition to coordinates, other useful data can be associated with each point, such as Red-Green-Blue (RGB) color or laser beam intensity. There are two main techniques through which point clouds can be generated: (1) photogrammetry and (2) LiDAR.

2.1. Imaged-based methods

Cost-effective cameras are easy to use to acquire images of an area of interest. The images can be processed in photogrammetry software to create a point cloud representation of the area. Photogrammetry methods are increasingly used thanks to a rise in computational power and the introduction of structure-from-motion (SfM) image progressing algorithms (Chandler, 1999; Eltner et al., 2016; Tannant, 2015). The structure-from-motion photogrammetry method allows for 3D reconstruction using stereo pairs of overlapping images and performs a bundle adjustment of many automatically located, corresponding points in each image. This results in the determination of the location and the orientation of the camera for each image and the 3D coordinates of points matched in the images (Eltner et al., 2016; Triggs et al., 2000). Unmanned aerial vehicles (UAVs) can be used to obtain stereo- and multi-view images and provide a rapid and inexpensive surveying tool for geoscience applications. To generate image-based point cloud data, integration of dense matching (Hirschmüller, 2005, 2008; Hirschmüller and Scharstein, 2007), multi-view stereovision (MVS) (Furukawa and Ponce, 2010; Nex and Remondino, 2014), and SfM (Snavely et al., 2006, 2008; Westoby et al., 2012) is required. The camera position and orientation and simultaneous multi-view image processing are accomplished through SfM. The dense matching and MVS algorithms create a large number of points in the point cloud (Xie et al., 2020). The SfM photogrammetry workflow typically has the following steps: (1) image acquisition, (2) image matching: recognition and matching of the corresponding points of overlapping photos, (3) reconstruction of image geometric data and the corresponding 3D coordinates of a sparse set of points in matched images using bundle adjustment, (4) densification of the sparse point cloud from reconstructed image geometry, and (5) geo-referencing (also applicable in step 2) (Eltner et al., 2016).

Structure-from-motion image processing can generate high-resolution point cloud data with good accuracy (Javadnejad et al., 2021; Martinez et al., 2021; O'Banion et al., 2018). Point cloud acquisition with high accuracy is particularly important for crack detection and damage assessment in construction projects (Martinez et al., 2021) and detecting rock mass features (joints).

The error sources of 3D reconstruction in SfM photogrammetry may include camera calibration, image blur due to platform motion, image resolution, image network geometry, image-matching performance, the texture of the surface, illumination conditions, and ground control point (GCP) accuracy and distribution (Bolkas, 2019; Eltner et al., 2016; Javadnejad et al., 2021).

2.2. LiDAR scanning

The LiDAR remote sensing method uses a laser beam to measure the distance (range) from the sensor to the targeted object under measurement. There are two different approaches to determining the range, the phase and pulse methods (Wehr and Lohr, 1999). The phase method provides more accurate and faster range determination, with the expense of having a limited range. In contrast, the pulse method, which is the most common method for remote sensing purposes, offers a wider range of measurements. Based on sensors and platforms, the resolution or the density of points may vary from ten to thousands of points per square meter (Qin et al., 2016). Concerning platforms, they are categorized into four main systems: terrestrial (TLS), airborne (ALS), unmanned (ULS), and mobile LiDAR scanning (MLS). A TLS mounted on a static tripod is used for close to middle-range conditions and can generate high-density point clouds. The point density for TLS can range from 50 to 10000 points/m^2, whereas, for ALS, it is typically 0.5 to 100 points/m^2 (Jaboyedoff et al., 2012b). Generally, ALS yields comparatively low-density point clouds since the sensor is flown at the highest distance from the ground. ALS point clouds tend to be the most expensive. MLS can be mounted on a moving platform, such as a car, and can be a suitable choice for providing 3D geospatial roadway information (Guan et al., 2016) for transportation-related applications (Toth, 2009). ULS systems installed on unmanned vehicles are relatively cheap compared to ALS and create point clouds with higher density due to their typically shorter measurement distance. ULS can be employed in various surveying tasks such as forestry, mining, and disaster monitoring (J. Li et al., 2019; Sankey et al., 2017; X. Zhang et al., 2019). Full-waveform LiDAR systems that sample the full return signal as a function of time can be used to accurately recognize scattered returns

from targets such as vegetation (Hancock et al., 2011, 2015). Fig. 1 summarizes the commonly used point cloud acquisition methods.

3. Segmentation techniques to extract planar surfaces from point clouds

The individual points in a point cloud can be separated into groups that share particular characteristics or belong to the same object. The process is often called segmentation, and it aims to facilitate the identification of intended regions as explicitly understandable features. Some point cloud properties make segmentation challenging. These challenges are illustrated in Fig. 2. All point cloud data are affected by some level of noise. This noise typically varies throughout a point cloud depending on acquisition geometry and surface properties. In addition, point clouds are often affected by outliers, which are data points that are geometrically inconsistent with the original surface (Wolff et al., 2016). Points in a point cloud are not uniformly spaced (Qi et al., 2017b), and some regions may be missing points. Downsampling can reduce this irregularity effect to some degree. There is no grid structure in a point cloud, as in a digital image, and in general, points do not have a natural order. Consequently, the relationships among neighboring points are not explicitly known, which results in a less efficient neighboring points search in an unstructured point cloud. (Qi et al., 2017a).

This section reviews various segmentation techniques deployed to extract planar segments from a point cloud (Fig. 3). The advantages and disadvantages of each method are also discussed. Then, the corresponding studies conducted to extract discontinuity planes from a rock mass point cloud are presented. In addition, some other relevant studies for extracting planar features from point cloud data in the literature are discussed. The goal is to highlight those methods that have not been applied on a rock mass point cloud but look promising.

The four main topics are discussed in the following section. First, edge-based methods that were first implemented on image data and then extended to 3D data are introduced. Next, region growing methods followed by surface fitting methods (Hough Transform and RANSAC) are discussed. Finally, unsupervised clustering-based methods are presented, and some of the commonly used algorithms to extract discontinuity planes are introduced.

3.1. Edge-based methods

The goal of edge-based methods is to identify the pixels on or close to regions with a significant local change in the intensity or color, defined as traces (radiometric-based edges). A rapid change in gray intensity number, an integer ranging from 0 (black) to 255 (white) of the data point, is a fundamental characteristic of edge-based methods for images (Nguyen and Le, 2013). Nevertheless, there are geometric-based edges (regions with high spatial gradients) where 3D coordinates are analyzed. These edge points can then be used to determine the shape of objects. To distinguish between the radiometric- and geometric-based edges in the point cloud data, we use the term “trace” for the radiometric-based edges and use the word “edge” for geometric-based edges in this work. Fig. 4 shows an image with numerous planar discontinuities, traces, and edges. Some of these are marked with a different color (planes indicated by a dashed closed polyline, traces are inside dashed red rectangles, and edges are shown with a yellow polyline).

The main steps in edge-based segmentation are (Rabbani et al., 2006): (1) detect edges to derive the borders of different regions, and (2) group points inside the boundaries as a common object. Bhanu et al. (1986) used a gradient-based method to fit 3D lines to data points and

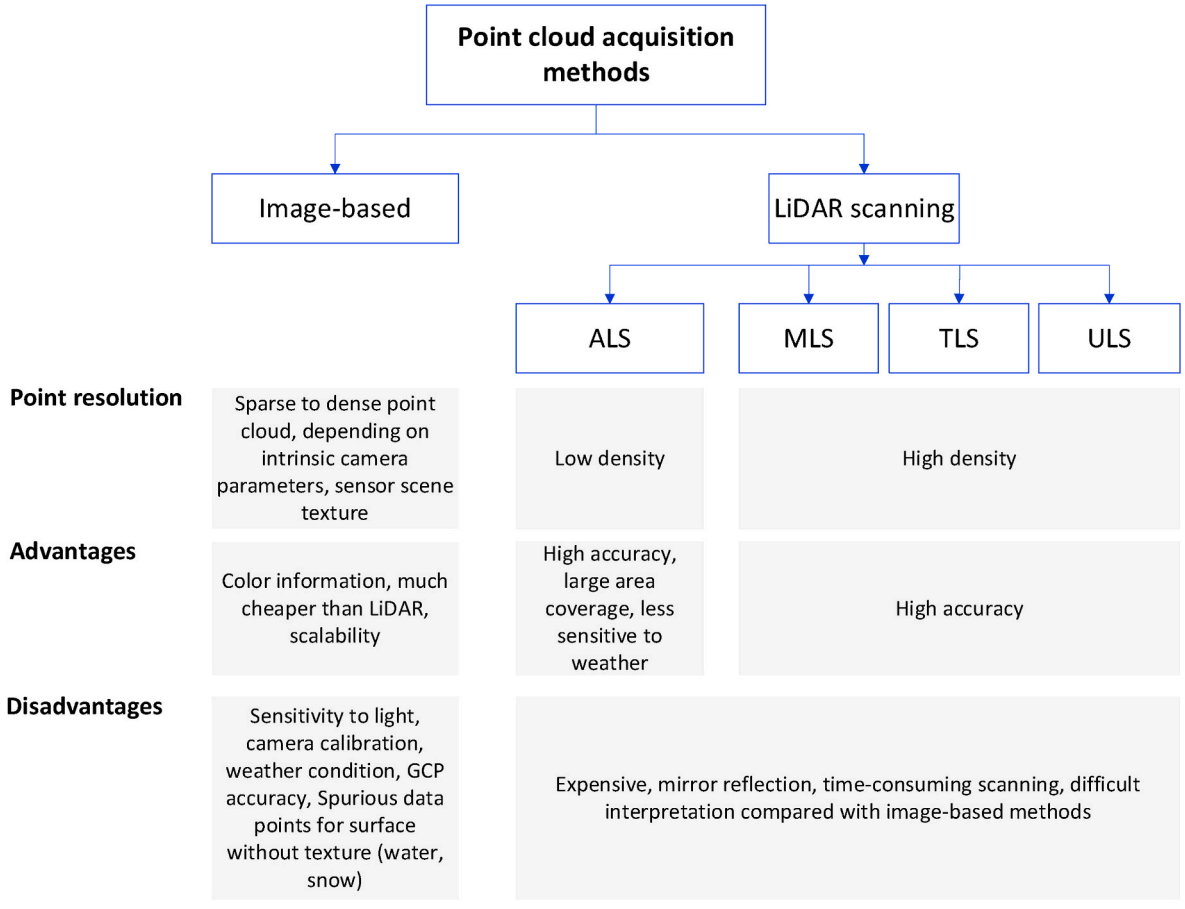

Fig. 1. Common point cloud acquisition methods and a summary of their characteristics.

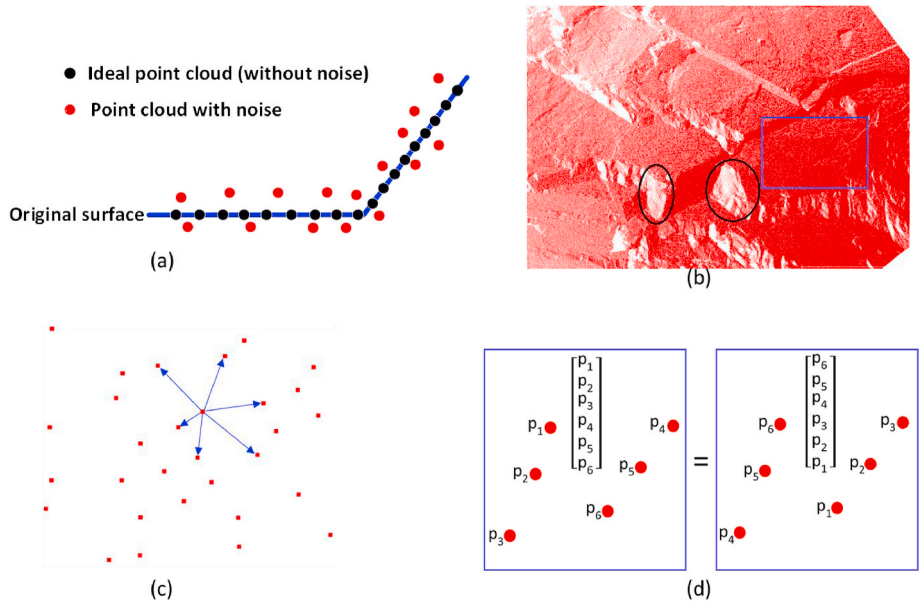

Fig. 2. Challenging properties of 3D point clouds, (a) Noise, (b) Varying point density (ovals highlight two low-density areas, a high-density area is highlighted by a rectangle; (c) unstructured, (d) Unordered.

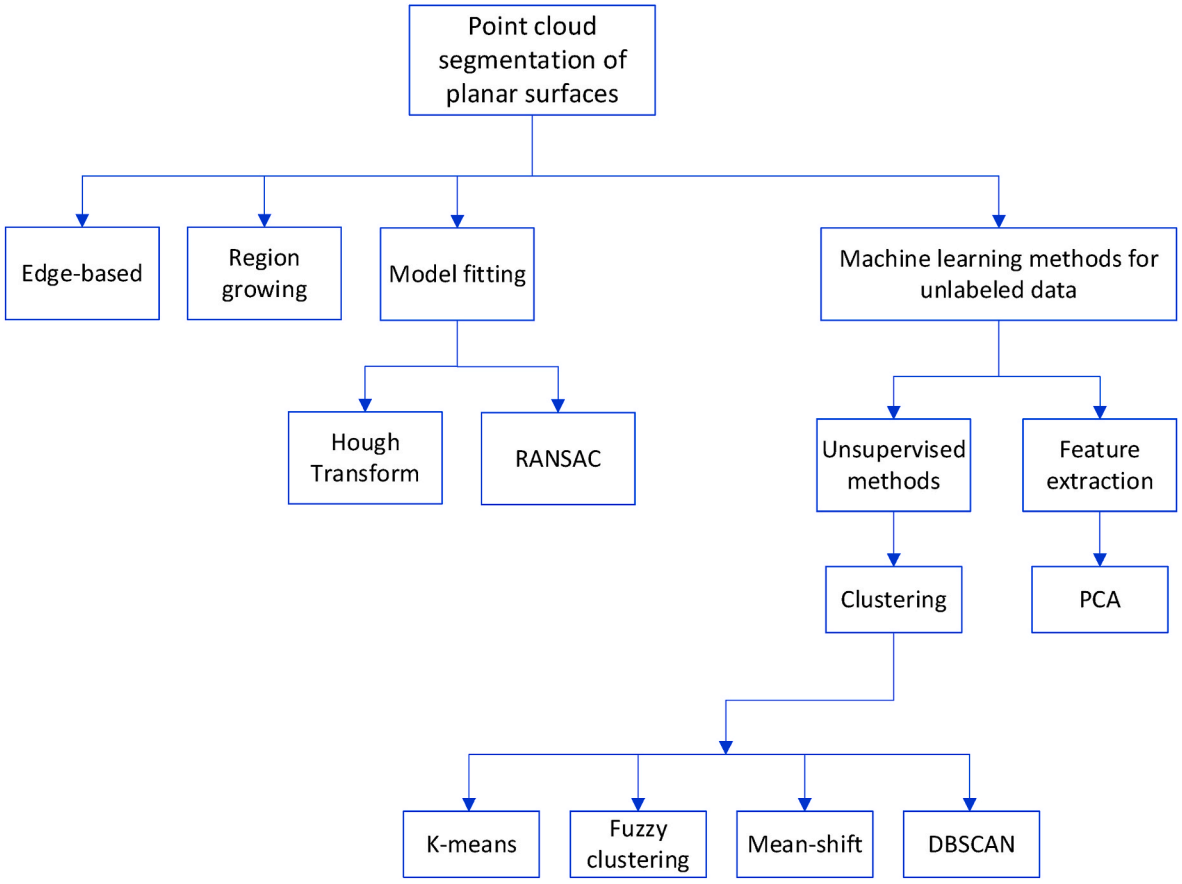

Fig. 3. Taxonomy of 3D point cloud planar surface segmentation methods.

monitored the variations in perpendicular directions to the surface (unit normal vector directions). A fast segmentation approach, in which the amount of data was reduced, was developed by Jiang et al. (1996). The method used high-level segmentation primitives. However, this method may not work well for a 3D point cloud with variable point density despite often being efficient and accurate.

Generally, edge-based algorithms deliver a fast segmentation of a point cloud because of their simplicity. They yield satisfactory performance when dealing with a dataset with an even density and low noise. However, such methods often end up with disconnected edges and poor

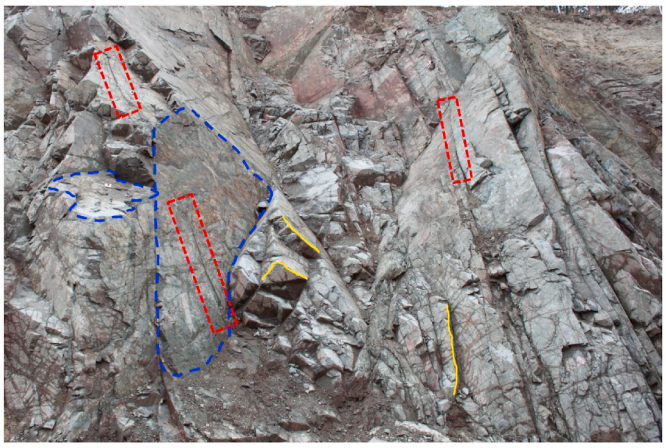

Fig. 4. Illustration of planes (blue), traces (red), and edges (yellow). (For interpretation of the references to color in this figure legend, the reader is referred to the Web version of this article.)

segmentation if no filling or interpretation techniques are used (Castillo et al., 2013; Grilli et al., 2017). This makes these methods inefficient for analyzing large datasets and dense point clouds (Xie et al., 2020).

Early attempts to automatically find discontinuity traces from digital images of a rock face were performed by Franklin et al. (1988) and Tanimoto et al. (1991). The resulting discontinuity traces were found to be insufficient and spurious. To improve the automatic tracing of discontinuities, Reid and Harrison (1997) considered a digital image of a rock face as a greyscale topographic surface on which light pixels reflect high elevation and dark ones as low elevation. They used the gradient and curvature of the surface, with an artificial topographic label at each pixel as the output on the intended discontinuity. Detecting and linking the labeled pixels in an appropriate manner resulted in the formation of the discontinuity trace. However, the traces detected by their algorithm were not satisfactory and only applied to a limited range of rock surface morphologies. Furthermore, Lemy and Hadjigeorgiou (2003) noted that binary images that emerge from segmentation contain pixels incorrectly associated with discontinuity traces, and filtering as a pre-processing stage is often required. They also argued that the optimal threshold value is not a convenient approach to building an automatic mapping tool. Therefore, algorithms such as those by Reid and Harrison (1997) are unreliable for obtaining the discontinuity traces from digital images of rock exposures, and only some discontinuities are detected.

Lemy and Hadjigeorgiou (2003) compared various edge and line detection methods and suggested a more efficient mapping procedure. The methodology follows the steps of (a) acquisition, (b) pre-processing, (c) segmentation, (d) representation, (e) recognition, and (f) interpretation. Depending on the intended complexity, these steps may be reduced to three main categories (Gonzalez et al., 2002). The semi-automatic detection for the trace length worked very well for limestone, while for carbonatite and granodiorite exposures, it was challenging to reach satisfactory results (Gonzalez et al., 2002).

Bolkas et al. (2018) investigated space-frequency transforms using LiDAR data to evaluate the effectiveness of those transforms in detecting discontinuities in a rock mass. They used several edge detection algorithms (Canny, Sobel, and Prewitt) to study the suitability of each for discontinuity detection. Wavelet, contourlet, and shearlet transforms were also compared. Contourlet and shearlet outperformed the other methods.

Similarly, Guo et al. (2018) presented an automatic methodology to detect discontinuity edges from 3D point cloud data using 1D truncated Fourier series and a Laplacian-based curvature-weighted smoothing technique to refine and thin the potential feature points. Lastly, the edge lines were developed using a feature-weighted line-growing algorithm. The different procedures are depicted in Fig. 5.

Maps of discontinuity traces were extracted by the fusion of a 3D point cloud and image data by Zhang et al. (2019). The 2D trace was derived using a hybrid local and global threshold method and image processing algorithms. The pixel locations of the detected traces were then linked to the 3D coordinates of a point cloud by transforming the

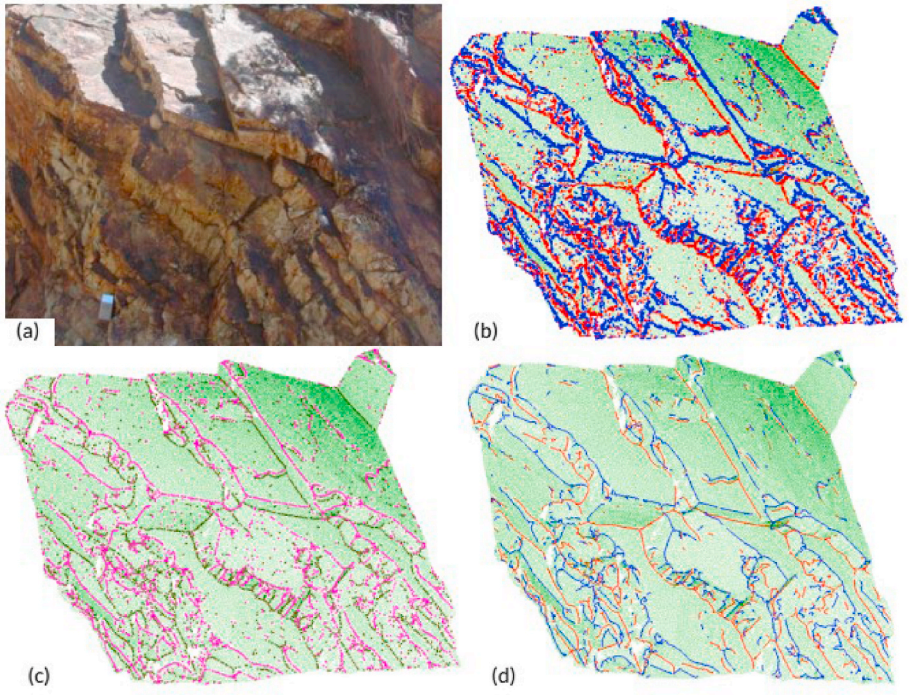

Fig. 5. (a) Image of the rock face (Lato et al., 2013), (b) Detected potential edge points (red and blue points), (c) Thinned edge points, and (d) Final edge lines (reprinted with permission from Elsevier (Guo et al., 2018)). (For interpretation of the references to color in this figure legend, the reader is referred to the Web version of this article.)

coordinates between the image and those of the point cloud. Finally, 3D spatial features of the traces were used to obtain the 3D discontinuity orientations.

3.2. Region-growing methods

A region-growing method was introduced for image segmentation by considering the color information of pixels around the neighborhood of a selected initial seed point (Xiao et al., 2013). A local search is performed through the k-nearest neighbors (knn) data points of a seed point to determine if an adjacent point should be added to the initial region. Later, this approach was extended to identify planes in 3D point clouds and define planar areas of building structures (Dong et al., 2018; Gorte, 2002; Hähnel et al., 2003; Nurunnabi et al., 2012; Rabbani et al., 2006; Vo et al., 2015; Xiao et al., 2013).

The region starts its growing procedure from a point with a low curvature value, or low local planar residual value, since it is located in a relatively flat area, and growth from this area reduces the total number of segments. A normal to a point is determined using a best-fit plane to a group of close points surrounding the point of interest. The angle is determined between the normals of a current seed point and an adjacent point. If the angle is less than a defined threshold value, the current point is added to the seed point, and the region of points belonging to the same plane grows. The output of this method results in clusters of points that should belong to the same roughly planar surface.

This method works best when the point cloud data are well organized. An organized point cloud corresponds to an arrangement where adjacent points in the file are spatially close to each other in the field, and this helps the nearest neighbor search procedures run more efficiently ("Point Cloud Library (PCL)," n.d.). The nearest neighbor search is the most crucial component of this algorithm, as it runs at each step of the growth (Xiao et al., 2013).

The location of the seeds and the growth criteria significantly affect the accuracy of region-growing algorithms. The seed locations and growth criteria need to be predefined and modified for each dataset, which introduces subjectivity into the process (Vo et al., 2015; Xie et al., 2020). The potential for inaccurate segmentation results is high if these methods are used for unstructured point clouds (Pu and Vosselman, 2006). Furthermore, these methods are computationally expensive, and a trade-off between accuracy and efficiency may be required (Xie et al., 2020).

The region-growing method was used to derive the discontinuity planes based on the variation of local surface normals or curvature (Wang et al., 2017). First, within the nearest neighbor search, a least-squares plane is estimated. The region growing is then applied by selecting the point with the minimum curvature as the initial seed point for the planar surfaces. Li et al. (2016) implemented a region-growing algorithm on a triangulated model of the point cloud data. They investigated four post-processing stages for discontinuity edge grouping, segment growth of the edge line, segment linkage, and removal of redundant edge points to obtain refined discontinuity edges. A disadvantage of this method is that the mesh size is required to be tuned (Li et al., 2016).

A modified region-growing method was used to improve the speed and efficiency of estimating the geometric parameters of discontinuities from point cloud data collected using LiDAR (Ge et al., 2018). The geometry parameters considered include orientation (using a normal vector of a discontinuity), spacing (estimating the distance between two planes), exposed area (using the dip angle of the discontinuity and projected area), and roughness (using fractal geometry). Two case studies of regular polyhedrons and a hydropower station tunnel were investigated in this work. The optimum threshold T, related to the difference between the normal adjacent points, was approximately 40° in the case study. However, finding a proper value for T can be a time-consuming task. The implementation of this study cloud be facilitated if a machine learning or optimization technique is used to estimate the optimum threshold T.

3.3. Surface fitting methods

3.3.1. Hough Transform

The Hough Transform (HT) in the image processing method (Hough, 1960) is used to detect geometric primitives within 2D images to extract lines and circles (Duda and Hart, 1972). Based on the 2D Hough Transform, a 3D Hough Transform was developed to detect surfaces such as planes, cylinders, and spheres within a 3D point cloud (Dube and Zell, 2011). HT operates by transforming the data to parameter space and finding clusters that correspond to geometric features in the point cloud (Tarsha-Kurdi et al., 2008a). To avoid the problem of the infinite slope, the Standard Hough Transform (SHT) (Duda and Hart, 1972) employs an angle-radius parametrization rather than the original form of slope-intercept (Xie et al., 2020).

The major disadvantage of this algorithm is its high memory consumption and computational cost (Kaiser et al., 2019), making it less popular for surface extraction for large point clouds. The method is also sensitive to segmentation parameters (Awwad et al., 2010; Tarsha-Kurdi et al., 2008b). Borrmann et al. (2011) reviewed various HT studies and presented a new accumulator design to improve HT performance by improving the efficiency of the voting process. HT-based methods in their review comprised the Standard Hough Transform (Duda and Hart, 1972; Illingworth and Kittler, 1988; Kälviäinen et al., 1995; Kiryati et al., 1991), Probabilistic Hough Transform (Kiryati et al., 1991; Matas et al., 2000; YlaJaaski and Kiryati, 1994), and Randomized Hough Transform (RHT) (Xu et al., 1990). The Randomized Hough Transform was the best choice for plane detection in a 3D point cloud because of its efficiency if there are only a few planes. While the processing time does not increase with the number of points in a 3D point cloud, it does with the number of planes. If there are over 15 planes in the dataset, the segmentation time required using the Randomized Hough Transform can be considerably longer than the region-growing method, as noted by Borrmann et al. (2011). It was also noted that the method requires a long processing time and a large amount of memory because of the need to store all parameters.

Recently, Limberger and Oliveira (2015) developed a deterministic 3D kernel-based Hough transform (3D KHT) technique for plane detection in unorganized point clouds. The 3D KHT method uses a fast technique to cluster coplanar points with a computational effort proportional to $n \log n$ (n is the points in point cloud data). Limberger and Oliveira (2015) reported that the technique was a few orders of magnitude faster than algorithms such as RHT and RANSAC for plane detection in a point cloud.

3.3.2. Random sample consensus

The random sample consensus (RANSAC) method is an iterative algorithm that estimates the parameters of a geometric primitive from a minimum number of points generating that primitive in a point cloud (Fischler and Bolles, 1981; Raguram et al., 2008, 2013). It is extensively used for shape detection (Nguyen and Le, 2013; Schnabel et al., 2007; Xu et al., 2016), including the identification of building façades (Adam et al., 2018; Bauer et al., 2003; Boulaassal et al., 2007) and roofs (Chen et al., 2014).

Plane construction in RANSAC starts by randomly choosing three non-collinear points and using these to define the parameters of the equation for a plane. This surface can be a plane. Next, other neighboring points are iteratively checked to see if they match the plane within a threshold level. Points that match the surface form a consensus set, and others are considered outliers. The surface model is dismissed if the consensus set contains only a few points and is kept if the consensus set is large.

RANSAC is computationally costly due to its randomness (Liu et al., 2019; Raguram et al., 2013) and its iterative nature (Xiao et al., 2013). The method is nondeterministic, and its main limitation is that spurious

planes can appear depending on the parameter values used to detect planes (Li et al., 2017; Limberger and Oliveira, 2015) (Fig. 6). To deal with this issue, one suggested solution is the use of MSAC (M-estimator sample and consensus) and MLESAC (maximum likelihood estimation sample consensus), which uses a loss function rather than a fixed threshold (Torr and Zisserman, 2000). Also, a soft threshold voting function with respect to two weight functions was developed to enhance the quality of the segmentation (Xu et al., 2016). The use of a threshold voting function is not efficient in large point clouds because a calculation of the normal at each point is required (Li et al., 2017).

While HT and RANSAC are powerful approaches, they come with downsides (Limberger and Oliveira, 2015; Maalek et al., 2018; Vo et al., 2015): (a) they may extract numerous spurious (false) planes that do not exist in the datasets; (b) the results of point cloud segmentation are sensitive to the positional accuracy of the point, point density, and noise; (c) they show poor performance when dealing with large datasets and/or complex geometries.

The two main merits of RANSAC-based algorithms are that they are robust to noise and do not require advanced optimization. RANSAC can deliver more successful object detection compared with the Hough transform methods (Tarsha-Kurdi et al., 2008b; Xie et al., 2020).

Within the last decade, numerous modifications to the RANSAC algorithms have been developed to enhance the accuracy, efficiency, and robustness of the method for identifying surfaces. These methods are presented in Fig. 7. The original diagram was proposed by Choi et al. (2009), and two additional methods (EVSAC (Fragoso et al., 2013) and GC-RANSAC (Barath and Matas, 2018)) were added by Xie et al. (2020) to this original illustration.

RANSAC can be used in various forms and extensions. An efficient approach to extract discontinuity plane orientations from rock mass point clouds is to apply RANSAC on clustering results from unsupervised machine-learning methods. As such, the randomness effect in RANSAC output is successfully controlled, leading to a more deterministic orientation estimation.

3.4. Unsupervised clustering-based methods

Clustering-based methods are considered unsupervised learning that categorizes points based on similarity in underlying structures, geometrical features, or spatial distribution. As opposed to surface fitting (RANSAC, Hough Transform), region-growing methods, and supervised-learning methods (Filin, 2001), the hidden patterns in clustering methods are not pre-assumed. In these methods, an array of similarity indexes with different features can be specified, such as normal vector, Euclidean distance, and density (Xu et al., 2018).

Some of the most common approaches for point cloud segmentation using clustering methods are K-means (Kuçak et al., 2017; Morsdorf et al., 2004; Sampath and Shan, 2006; Shahzad et al., 2012; Zhu and Shahzad, 2014) and its variants, fuzzy clustering (Guo et al., 2017; Kong et al., 2014; Sampath and Shan, 2010), and mean-shift (Ximin et al., 2015; Zhang et al., 2018). There are also methods in which the Density-Based Spatial Clustering of Applications with Noise (DBSCAN) algorithm is employed to conduct the clustering (Aljumaily et al., 2017; Gélard et al., 2017; Wang et al., 2019).

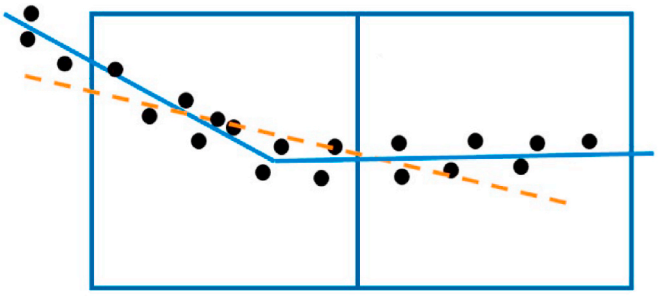

Fig. 6. Two well-estimated hypothetical planes are shown in blue, and a spurious plane in orange is generated using the same threshold (reprinted from (Li et al., 2017)). (For interpretation of the references to color in this figure legend, the reader is referred to the Web version of this article.)

Table 1 summarizes the characteristics of the common unsupervised machine-learning algorithms that are discussed in this section of the paper.

3.4.1. K-means algorithm

The K-means algorithm is a popular data clustering algorithm that starts with a collection of randomly selected initial centers. Each data point is placed in a cluster based on the computed distance between the point and each cluster center. It then assigns that point to the cluster whose center is closest. This algorithm is simple and relatively fast. It can handle large datasets, including nominal and numerical data, and it is adaptable to sparse data. A significant disadvantage is that this algorithm is sensitive to noisy data points, and it requires the number of clusters to be preset.

The K-means algorithm is prone to converge to local minima and is slow for high-dimensional data. The randomness of initial partitions can yield dissimilar clusters, and it does not deliver accurate results if clusters have non-convex or non-spherical shapes (Fränti and Sieranoja, 2019; Xu and Tian, 2015). Yu et al. (2020) developed a tri-level and bi-layer K-means algorithm to address its noise and initialization sensitivity, and they reported higher accuracy compared with classic K-means. In a recent study (Sinaga and Yang, 2020), a novel unsupervised K-means (U–K-means) was proposed to automate the initialization by defining an entropy penalty term for bias control and choosing an optimum cluster number using a learning schema. Using a newer version of the K-means algorithm may improve the extraction of discontinuity planes from a point cloud. The traditional K-means needs to be associated with other methods to handle noise, initialization, and the spherical shape of clusters.

Chen et al. (2016) studied the automatic extraction of discontinuity orientations from a rock mass point cloud. Their method consisted of four main steps. First, they grouped the discontinuity sets by employing the K-means clustering method. Second, the discontinuities were segmented and optimized. Third, using the RANSAC method, the best-fit discontinuity planes were found. Finally, the coordinates of the discontinuity planes were transformed. Case studies were used to evaluate the method.

Using point cloud data acquired from photogrammetry, Li et al. (2019) developed a graphical user interface (GUI) tool using MATLAB in which five discontinuity parameters are extracted from a point cloud of a rock mass. The orientation, aperture, edge, spacing, and roughness of discontinuities were derived. They used improved K-means to group the discontinuity sets and a RANSAC plane fitting method to determine the planar surfaces.

3.4.2. Fuzzy clustering

A modified version of K-means, known as soft clustering, works in a continuous interval of 0–1 to express the relationship of a sample point to a cluster. The fuzzy C-means clustering (FCM) algorithm is frequently used in pattern recognition. The method is capable of assigning each data point to multiple clusters. Some advantages of the method are that it is computationally efficient, only needs a single parameter of bandwidth size, and it is robust to outliers. The disadvantages of the method include relatively low scalability, and the solution can be trapped in a local rather than regional optimal. The method is also sensitive to the hyperparameter values, and the number of clusters must be preset.

A revised fuzzy C-means (RFCM) (Askari, 2021) method was proposed to deal with noisy data and clusters of different sizes and densities and remove cluster overlap. This extension of FCM can be a suitable approach for a rock mass point cloud as it can address noise, point density variations, and both the size of the point cloud and clusters of

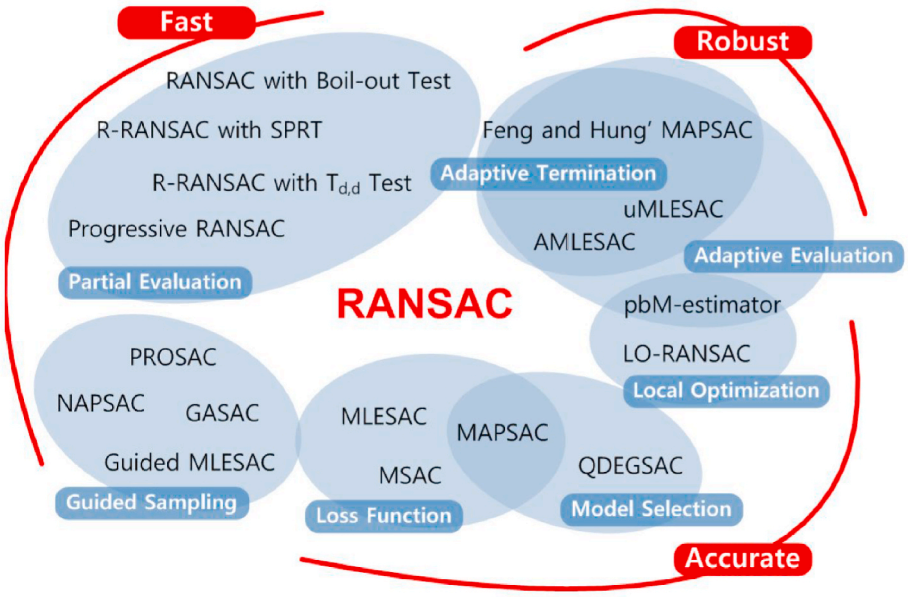

Fig. 7. RANSAC algorithms are categorized according to their performance and basic techniques (reprinted with permission from (Choi et al., 2009)).

Table 1
Comparison of common unsupervised machine-learning algorithms (notation O describes the relationship between the time complexity and the number of inputs, n).

	K-means	FCM	Mean-shift	DBSCAN
Computational time	O(n)	O(n)	O(n log n) to $O(n^2)$	O(n log n) to $O(n^2)$
Initialization problem	yes	yes	no	no
Noise sensitive	high	moderate	low	low
Stability (sensitive to input data)	high	moderate	little	moderate
High-dimensional data	no	no	no	yes
Scalability	moderate	moderate	low	low
Cluster shape	convex	convex	arbitrary	arbitrary

point clouds.

Guo et al. (2017) studied semi-automatic analysis of rock mass discontinuity orientation from a 3D point cloud. They prepared the data for segmentation by removing outliers first. The point cloud was divided into subsets, considering various parameters such as the normal vector and discontinuity dip and dip direction. The firefly algorithm (FA) and the fuzzy c-means (FCM) algorithm were used to cluster points based on their normal vectors. In the end, clusters belonging to each discontinuity set were merged and colored for better visualization.

3.4.3. Mean-shift algorithm

The mean-shift algorithm is a moving window-based approach to assign the data points to the cluster centroid by shifting them towards the dense area of data points. Unlike the K-means algorithm, a mean-shift does not require the number of clusters to be set in advance. The mean-shift algorithm determines this number for the given data. The key parameter in this algorithm is the bandwidth size of the kernel used. An important advantage of the method is that the number of clusters does not need to be predefined. The method can handle point clouds of any shape, needs only a single parameter of bandwidth size, and is robust to outliers. The disadvantages of the method are that the output depends on bandwidth size, and its selection may not be trivial.

The mean-shift algorithm is relatively slow, especially for large datasets, and has poor scalability with high-dimensional data. The computation time for this algorithm is generally O(n log n) to $O(n^2)$. This algorithm clusters discontinuity sets using normal vectors of points better than other algorithms when used in their classic form (Comaniciu and Meer, 2002; Xu and Tian, 2015).

Zhang et al. (2018) performed automatic detection of discontinuities in a 3D digital surface model (DSM) of a rock mass. A mean-shift clustering algorithm was used to identify and classify the orientation and position of discontinuity planes. Then, a region-growing algorithm was used to extract the corresponding feature planes. This method eliminated spurious points in a point cloud related to vegetation and may directly extract planar features such as joints.

3.4.4. Density-based spatial clustering of applications with noise (DBSCAN)

DBSCAN is a non-parametric algorithm that begins with a random starting point (p). A radial distance is defined to form a neighborhood for the selected starting point. If there are a minimum number of points (MinPts) within this radius, point p is defined as a core point. When the number of points in a defined neighborhood is smaller than the value of MinPts, this point is defined as a border point. A core point with all points within the radial distance creates a cluster. Each core point that is not within a cluster forms a new cluster.

While similar to the mean-shift algorithm, DBSCAN has remarkable advantages. As opposed to the mean-shift algorithm, which places outliers in a cluster, DBSCAN is robust to noise and is capable of identifying outliers as noise. The method also finds arbitrarily sized and shaped clusters comparatively well. Another advantage of DBSCAN is that the number of clusters does not need to be preset.

In dealing with hierarchical clusters, DBSCAN cannot efficiently handle datasets with highly variable point densities. In this case, a hierarchical density-based clustering method may be used. Ordering points to identify the clustering structure (OPTICS) (Ankerst et al., 1999) and Hierarchical-DBSCAN (HDBSCAN) algorithms are examples of this method (Campello et al., 2013). Another disadvantage of DBSCAN is the difficulty of estimating an appropriate distance threshold with high-dimensional datasets.

The orientation and position of rock mass discontinuities from 3D LiDAR point cloud data were derived using a semi-automatic procedure by Riquelme et al. (2014). Their procedure involved: (1) normal vector estimation of discontinuity planes using principal component analysis (PCA), (2) coplanarity test to remove anomalous points, (3) semi-automatic detection of discontinuity sets by KDE (kernel density estimation) analysis, assigning each point to a group of discontinuity set

through the distribution patterns, and (4) automatic extraction via a density-based clustering algorithm for single discontinuities. It was highlighted that a solid background in rock mechanics combined with field images is required for the optimal application of this method. Fig. 8 illustrates the scanned area and the corresponding segmented 3D point cloud showing each discontinuity set in a different color. In subsequent work, a discontinuity spacing study using a 3D point cloud was carried out by Riquelme et al. (2015). This method requires the 3D dataset to be pre-classified, reflecting that discontinuity sets are extracted, and each point is labeled with the related discontinuity set. Three case studies were considered in their work using laser scanning and synthetic data. They reported that their method's results on discontinuity orientation estimation are reasonably close to those obtained through manual measurements.

Singh et al. (2021) presented automated discontinuity extraction from a point cloud. As the first step, several filtering methods were applied to remove the vegetation from the raw point cloud. They defined five descriptors, namely eigenvalue descriptor (EVD), radial surface descriptor (RSD), fast point feature histogram (FPFH), normal, and curvature, on which K-Medoids clustering was implemented to obtain the discontinuity sets. Then, DBSCAN was performed to separate each discontinuity plane. It was reported that the proposed method might provide reliable results in a complex environment.

3.5. Principal component analysis method

Principal component analysis (PCA) is a statistical technique that, with emphasis on variation, identifies strong patterns in a dataset using an orthogonal transformation. PCA is a common method to detect local planar surfaces and linear points in a 3D point cloud. It converts a set of potentially correlated variables into several linearly independent (uncorrelated) variables referred to as principal components. The regular PCA forms a covariance matrix that is decomposed into eigenvalues and eigenvectors. The purpose is to capture the dataset variation and transform it into independent orthogonal axes (three axes are possible for a 3D point cloud).

For planar surface segmentation of a point cloud, K-nearest neighbors are calculated for each point in a point cloud. Next, a least-square local plane is fitted to the local neighbors of the point. The usual method to estimate the normal vector for each point is to apply PCA (Hoppe et al., 1992). The covariance matrix, $C_{3\times3}$, can be written as:

$$C_{3\times3} = \frac{1}{k}\sum_{i=1}^{k}(p_i - \overline{p})^T(p_i - \overline{p}); \quad \overline{p} = \frac{1}{k}\sum_{i=1}^{k} p_i \tag{1}$$

where p_i is the local centroid of the k-neighborhood of the point p. Applying a Singular Value Decomposition (SVD) on $C_{3\times3}$, the eigenvectors ($v_1, v_2,$ and v_3) and the corresponding eigenvalues, $\lambda_3 \leq \lambda_2 \leq \lambda_1$, can be obtained.

The normal vector is estimated as the eigenvector (v_3) corresponding to the smallest eigenvalue (λ_3). The three eigenvalues represent an ellipsoid that defines a local 3D data distribution. The smaller λ_3 is the variance of deviations from the best-fit plane ($\lambda_1 \cong \lambda_2 \gg \lambda_3$). In the case $\lambda_1 \gg \lambda_2, \lambda_3$, the ellipsoid represents a linear feature (edge, border, etc.), and when $\lambda_1 \cong \lambda_2 \cong \lambda_3$, the ellipsoid is closer to a sphere (Mallet et al., 2011).

The eigenvalues can be used to define eight local 3D shape features (Mallet et al., 2011; Pauly et al., 2003; Toshev et al., 2010; Weinmann et al., 2015; West et al., 2004), which are listed in Table 2. These are common eigenvalue-based shape features representing the local spatial distribution of points in a point cloud.

The variation in the values of λ_3 in a region of points yields an estimate of the local noise level or surface roughness as a deviation from the fitted plane. The concept of surface variation or curvature (σ_k) is defined in Table 2 (Pauly et al., 2002, 2003). The parameter σ_k will be zero if all the neighbor points perfectly fit a plane.

3.6. Methods for improving normal vectors and edges

The PCA technique performs accurately if the neighboring points exist on a smooth surface. Despite being a fast approach, calculating a normal to a point becomes erratic at corners and edges and in the presence of outliers. Thus the classical PCA does not work well for point clouds with noise and in the vicinity of geometric singularities (Khaloo and Lattanzi, 2017; Maalek et al., 2018; Nurunnabi et al., 2015). This challenge is shown in Fig. 9. (a) Challenges with estimating normal vectors (reprinted with permission from Elsevier (Khaloo and Lattanzi, 2017)), (b) Example of a rock cliff with horizontal and vertical discontinuity planes perpendicular to the rock face (Athabasca River, Alberta, Canada) 9(a) and is discussed by Khaloo and Lattanzi (2017) in terms of point cloud analysis of civil infrastructure. This is important for point clouds of rock mass structures where geometry variation and topography can be highly irregular.

Despite the limitations of PCA, many researchers have used PCA combined with other techniques to extract planar surfaces (Ballast, 2007; Belton and Lichti, 2006; Bosché and Biotteau, 2015; Bremer et al., 2013; Filin and Pfeifer, 2006; Kim et al., 2007, 2016; Maquet, 2010; Pu and Vosselman, 2006; Rottensteiner et al., 2005; Su et al., 2016; Tovari and Pfeifer, 2005; Wang et al., 2015) and sharp edges (Bazazian et al.,

Table 2
Geometric features based on the eigenvalues.

Sum	$\lambda_1 + \lambda_2 + \lambda_3$
Omnivariance	$\frac{1}{(\lambda_1 \bullet \lambda_2 \bullet \lambda_3)^{\frac{1}{3}}}$
Eigenentropy	$-\sum_{i=1}^{3}\lambda_i \bullet \ln(\lambda_i)$
Anisotropy	$(\lambda_1 - \lambda_3)/\lambda_1$
Linearity	$(\lambda_1 - \lambda_2)/\lambda_1$
Planarity	$(\lambda_2 - \lambda_3)/\lambda_1$
Surface variation	$\lambda_3/(\lambda_1 + \lambda_2 + \lambda_3)$
Sphericity	λ_3/λ_1

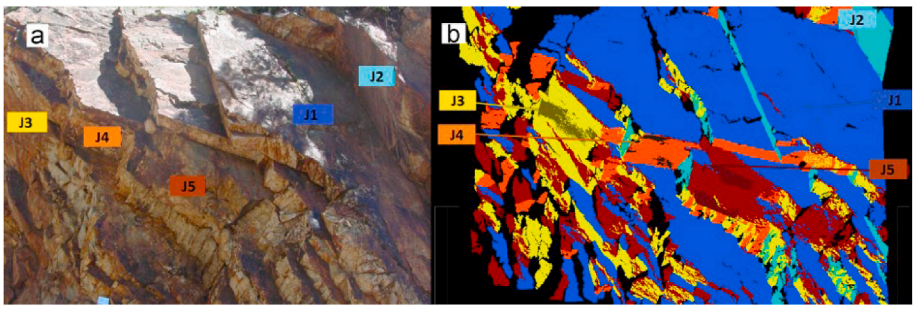

Fig. 8. (a) A section of the scanned area (Lato et al., 2013), (b) Segmented 3D point cloud showing colored points assigned to five discontinuity sets (J1, J2, J3, J4, and J5), with black points not associated with a discontinuity set (reprinted with permission from Elsevier (Riquelme et al., 2014)).

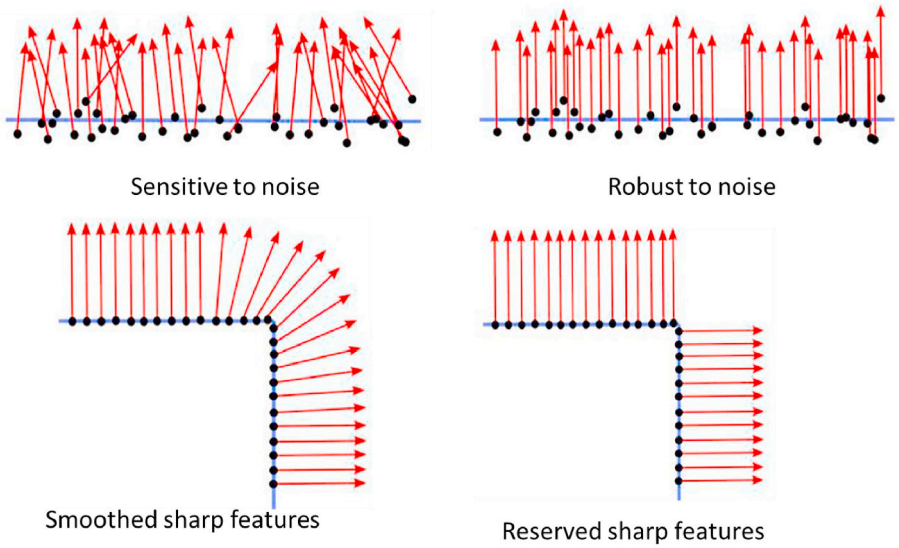

(a)

(b)

Fig. 9. (a) Challenges with estimating normal vectors (reprinted with permission from Elsevier (Khaloo and Lattanzi, 2017)), (b) Example of a rock cliff with horizontal and vertical discontinuity planes perpendicular to the rock face (Athabasca River, Alberta, Canada).

2015; Gumhold et al., 2001). For example, Nurunnabi et al. (2014) demonstrated that robust-PCA achieves efficient and accurate surface normal results. Similarly, Khaloo and Lattanzi (2017) found that sharp edges are maintained, and the segmented surfaces properly reflect the actual geometry of the physical object.

Statistical approaches are commonly used to minimize the effect of outliers by estimating model parameters. MVE (minimum volume ellipsoid) and MCD (minimum covariance determinant) are two popular robust multivariate dispersion estimates. The MVE has a low convergence rate and is not very efficient (Nurunnabi et al., 2014). In contrast to MVE, MCD embodies several merits. MCD is more statistically efficient because of being an asymptotically normal estimator (Seheult et al., 1989). It has higher accuracy and a higher convergent rate. Furthermore, MCD is affine equivariant, resulting in the estimator being independent of the measurement scale (Hubert et al., 2012). This makes an MCD estimator a better choice for point cloud processing purposes

(Maalek et al., 2018). There are two common MCD estimators, namely fast-MCD and deterministic-MCD (Det-MCD). Det-MCD is permutation invariant because the results do not rely on the order of the data, whereas fast-MCD is not. Furthermore, Det-MCD is reported to be faster than fast-MCD while being equally or even more robust than fast-MCD (Hubert et al., 2012; Nurunnabi et al., 2012). Thus, more accurate planar or linear clustering results are anticipated for robust-PCA when using Det-MCD. More details about Det-MCD are found in Hubert et al. (2012). The results suggest that DetRD-PCA and DetRPCA methods outperform and correctly identify the edges at the top and bottom of the point cloud (Nurunnabi et al., 2014). As for planar surface segmentation, DetRD-PCA and DetRPCA yield better performance, each with only one over-segment (OS) area and no under-segment area.

3.7. Summary, challenges and solutions

This sub-section summarizes the segmentation techniques introduced in Section 3 and presents some challenges and potential solutions. Four approaches for planar surface segmentation of point clouds were discussed in this section. Some are based on a mathematical model using geometry and spatial analysis (i.e., region growing and model fitting) along with estimators to match linear/nonlinear models to point data (Nguyen and Le, 2013). These methods can reach a satisfactory outcome for non-complex scenes. However, limitations include difficulty selecting the model size while fitting objects, noise sensitivity, and the methods may not work well for complex geometries. The other approach uses machine-learning techniques to explore 3D features using feature descriptors to learn different object type classes from point cloud data. Then they apply the knowledge learned to classify the data (Nguyen and Le, 2013). Machine-learning techniques generally yield better performance than geometry-based techniques for complex point clouds. This is because point cloud data often contains noise, variable point density, and occlusions, which are better handled by machine-learning techniques.

An accurate normal estimation in a point cloud plays a crucial role in properly segmenting the intended plane features. Applying PCA on a point cloud may result in satisfactory normal vector calculation for each point if proper procedures are applied to remove or modify the outlier data points or edges and boundaries with a rapid change in curvature. Some interesting methodologies discussed in Section 3.6 can correct normal vectors to better segment planes and edge points and reduce under-/over-segmentation. The recently introduced modified PCA methods are a promising approach, but no studies have been published in the literature on their applications to rock mass point clouds. Also, to properly detect discontinuities in a rock mass point cloud, methods should be deployed that can adapt to irregular and frequent changes in surface orientations to preserve the boundaries and edges of the plane surfaces and show robustness to noise.

A common issue of geometry-based methods for discontinuity extraction is that they fail to properly recognize discontinuity planes that are perpendicular to rock faces, which are only exposed as traces (Menegoni et al., 2019) or those with slight curvature changes (Guo et al., 2019; P. Zhang et al., 2019). Menegoni et al. (2019) found that dominant bedding planes perpendicular to a rock slope face were not recognized. They reported that a lack of consideration of these discontinuities might lead to misinterpretation of potential rock failure modes. Fig. 9(b) presents an example of discontinuity planes perpendicular to a rock face. Two samples from horizontal and vertical planes are depicted. These plane exposures are traces on the rock face and often remain undetected by geometry-based methods. For detecting such discontinuities, color information (RBG or intensity) is required and should be used along with the XYZ coordinates. For a point cloud with color information, calculating the color gradient can recognize the trace of discontinuities perpendicular to the rock face.

4. Comparison of different methods

In this section, two point cloud datasets are introduced and used to compare the implementation of some of the methodologies presented in Section 3. The segmentation results for planar discontinuities in rock mass point clouds are qualitatively (visually) and quantitatively discussed and compared.

Researchers have frequently used the first introduced rock mass point cloud dataset (PC1) in the field of artificial intelligence. They assessed their developed methodologies using commonly accepted performance metrics for segmentation. Their evaluation was performed for individual planes and/or the whole point cloud by comparison with a 'ground truth' point cloud.

The geotechnical and geological engineering community frequently uses the second rock mass point cloud dataset (PC2). Two sets of ground truth orientations were introduced, and various automated workflows were developed to estimate the orientation of planes within this point cloud. Our research presents a new set of ground truth plane orientations. The semi-/automated orientations results found in previous studies are compared with the ground truth orientations.

4.1. Rock surface point cloud datasets

Point cloud 1 (PC1) was acquired using a Leica HDS600 scanner near Kingston, Ontario, Canada. Point cloud 2 (PC2) represents a quarzitic rock cut captured using an Optech scanner near Ouray, Colorado, USA. These two point clouds originate from the Rockbench repository (Lato et al., 2013). Fig. 10 shows a front photo and the corresponding trimmed point cloud for the two rock surfaces. The size and the average density of the point clouds are listed in Table 3.

4.2. Performance metrics

The point cloud segmentation performance may be examined using evaluation metrics such as precision, recall, and F1 (Vo et al., 2015). The results can be visualized by forming a confusion matrix in which the ground truth labels (i.e., the points belonging to a specific plane) are compared with the model prediction.

Accuracy is the ratio of correctly predicted observations (data points) to total data points, as shown in Equation (2). Precision represents the portion of correctly predicted positive observations (data points) relative to the total positive data points, as defined in Equation (3). Recall is the portion of correctly predicted positive observations (data points) to all data points in the actual class, as defined in Equation (4). The F1 score is a balance between precision and recall, defined in Equation (5). Another performance metric, intersection over union (IOU), is used for various tasks such as segmentation, tracking, and detection. It is defined as the intersection size between the ground truth and the model estimation over the sum of the ground truth and the model estimation sizes. IOU shows more sensitivity towards false detections as it considers FN and FP in its calculation (Equation (6)). When the IOU reaches equal or greater than 0.5, the prediction is usually assumed to be correct.

$$Accuracy = \frac{TP + TN}{TP + FP + FN + TN} \tag{2}$$

$$Precision = \frac{TP}{TP + FP} \tag{3}$$

$$Recall = \frac{TP}{TP + FN} \tag{4}$$

$$F1 = 2 \times \frac{Precision \times Recall}{Precision + Recall} \tag{5}$$

$$IOU = \frac{TP}{TP + FN + FP} \tag{6}$$

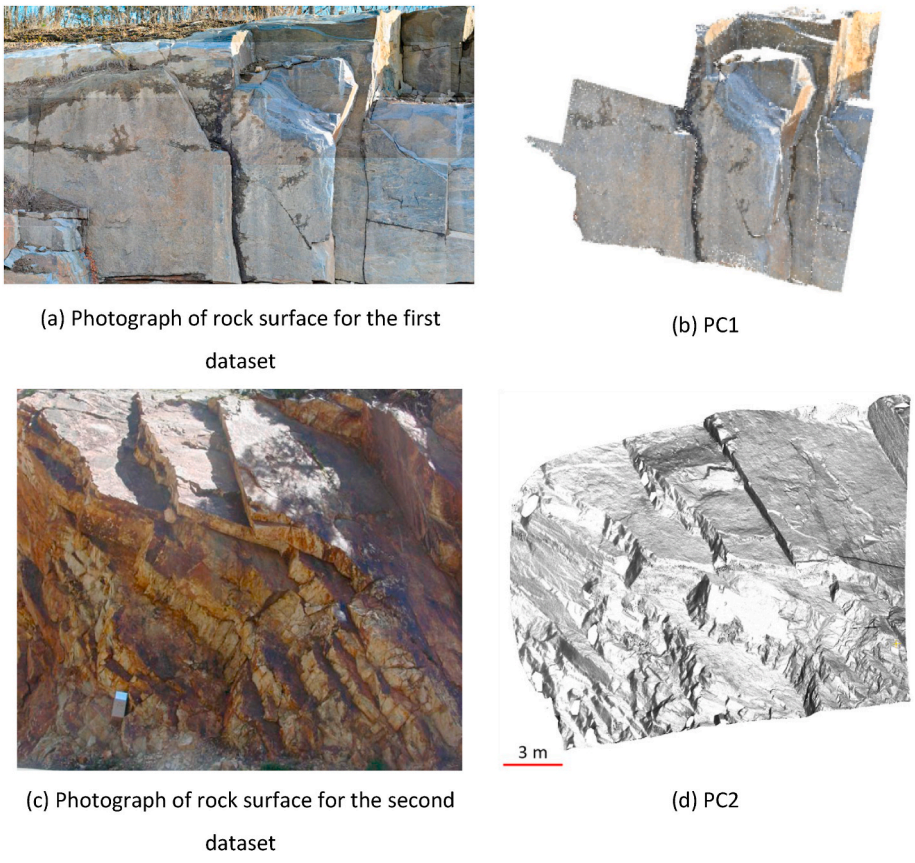

Fig. 10. (a) Photograph of rock surface for the first dataset (Lato et al., 2013), (b) First point cloud (PC1), (c) Photograph of rock surface for the second dataset (Lato et al., 2013), (d) Second point cloud (PC2).

Table 3
Basic information about rock mass point cloud data.

Name	Number of points	Average point spacing (cm)	Bounding box size (m)
PC1	387,610	4	48.86 × 36.04 × 14.19
PC2	1,024,521	2	29.29 × 25.85 × 22.88

4.3. Results for hybrid methods

Many research studies combine segmentation techniques to use each method's advantages. In this subsection, two main groups of studies are presented. The first group (Section 4.3.1) evaluates discontinuity plane segmentation in rock mass point clouds based on the performance metrics introduced in Section 4.2. The second group analyzes the quality of the orientations calculated for the segmented discontinuity planes (Section 4.3.2).

4.3.1. Segmentation performance

Leng et al. (2016) combined HT and RG (HT-RG) to segment the rock mass planes. Instead of using a standard HT, a clustering-based procedure for the voting distribution in the parameter space was used. HT-RG can detect discontinuity planes with different sizes, and the overall segmentation precision was around 91%. However, it may miss detecting the small and low-density plane surfaces, is inclined to over-segmentation, and its computation time is relatively high.

Liu et al. (2019) presented a three-step methodology (MOE). (1) Spatial grid for voxelization was performed, followed by coplanar clustering based on an analysis of the eigenvalues in the covariance matrix. This step segments the point cloud into three voxel types: coplanar, non-coplanar, and sparse voxels. (2) Major orientation for normal vectors of coplanar voxels was estimated using the bivariate Gaussian kernel. (3) Finally, the seed voxels were selected based on major orientations, and a voxel-based region-growing method was applied to extract the surface cluster sets. The sub-surfaces of each cluster are coplanar and a single plane surface can be defined and extracted from other coplanar and non-adjacent surfaces.

RHT, region growing, and RANSAC were implemented with C++ code using the PCL library (Rusu and Cousins, 2011). Similarly, an optimized RANSAC (Schnabel et al., 2007) was implemented using the Computational Geometry Algorithms Library (CGAL). MOE implementation is fast, can detect the planes with good accuracy (92% for precision), and preserves the boundaries. However, similar to HT-RG, it may miss detecting the small and low-density plane surfaces. Also, a large number of parameters need to be tuned.

In a similar attempt, RANSAC with voxel-based RG (RAN-RG) was used to extract the planes from a point cloud (Hu et al., 2020). First, normal vectors were estimated using the covariance matrix formed after applying PCA. Then, the point cloud was voxelized, and a coplanarity test on each voxel produced in the previous step was performed. The optimum plane in each voxel was selected as the growth unit for RG in the next step. The performance metrics for this method (91% for precision) are similar to those obtained by MOE. While the computation cost in this method (RAN-RG) is slightly higher than MOE, the results seem less prone to over-segmentation than MOE.

RAN-RG was modified by introducing the supervoxel concept (Supervoxel-RG) (Yu et al., 2020) to improve rock mass point cloud segmentation results. Supervoxel segmentation is designed after a coplanarity test and edge information extraction to obtain the growing units. The RG method is split into smaller subtasks for more accurate segmentation results. The computation time for this method is higher

than RAN-RG and MOE. It is also inclined to over-segmentation and occasionally leaves holes in the segmented plane. However, the reported results suggested a slightly better accuracy in the segmentation of planes.

Qualitative comparisons of the results for two point cloud datasets are presented for PC2 in Fig. 11 and for PC1 in Fig. 12. The segmentation results suggest that RHT, RG, and RANSAC have poor performance (detecting spurious planes and over-segmenting) when segmenting the planar surfaces, particularly for PC2 shown in Fig. 11, which has various challenges such as data gaps, low-density areas, and smaller plane sizes. While the optimized RANSAC outperformed the RANSAC, it yielded some over-segmented planes. HT-RG could not detect small planes and removed data points in areas with sparse density and the edges of planes.

DSE and the voxel-based method (MOE) generally achieved better results. However, DSE and MOE removed the sparse-density plane areas in the segmentation. Comparing the segmentation results for PC2 using DSE originally presented by Riquelme et al. (2014) (see Fig. 8b) and those presented in Fig. 11(g) (Liu et al., 2019) suggests that the segmentation results in Fig. 11(g) may not represent the best results using DSE.

Segmentation results of PC1 for ground truth data, shown in Fig. 12 (a), and different methods in Fig. 12(b)–(j) are illustrated. Red polygons reveal deficiencies in the results. An ellipse indicates over-segmentation, a rectangle represents scattered data points in the plane, a parallelogram represents incorrect results, a rhombus represents a bad boundary, and a trapezoid represents missing detection (Liu et al., 2019). The black areas in Fig. 12 correspond to non-coplanar points, and other colors each shows an individual planar surface. Red polygons are used to highlight the deficiencies in the results for each method. RHT and the optimized RANSAC resulted in over-segmented planes. They also assigned scattered points on some planes to the wrong cluster. RG results were partly incorrect with over-segmentation planes detected. The shortcomings of RANSAC results are over-segmentation, inaccurate plane boundaries, and scattered points. The results for HT-RG and DSE were found to over-segment and miss small and low-density surfaces in PC1. The voxel-based results by Liu et al. (2019) generally showed satisfactory results compared to other methods. However, it misses areas with low density and smaller surfaces. The relative computation time, advantages, and deficiencies of these methods and their overall performance are quantitatively compared for PC1 in Table 4.

4.3.2. *Discontinuity plane orientations for PC2*

Chen et al. (2016) studied the automatic extraction of blocks of rock from a 3D point cloud using a modified RANSAC method combined with an estimation of the discontinuity intersections. One advantage of this approach is that the extraction uses the raw point cloud rather than a triangulated mesh. This reduces the processing time to extract features such as the size and volume of the blocks.

In recent work by Kong et al. (2020), a density-based approach (Zhu et al., 2016) was used to segment discontinuities from rock mass point clouds. Unlike DBSCAN, this approach is not sensitive to point cloud data with varying densities and handles noisy data points better. Clustering of discontinuity sets was performed using the CFSFDP (Clustering by Fast Search and Find of Density Peaks) algorithm (Rodriguez and Laio, 2014) and iterative estimation of Fisher's K-value (Kulatilake, 1985; Slob, 2010) to remove noisy data points. The RANSAC method was also used to fit the discontinuity plane. Two case studies on rock slopes were used to demonstrate this procedure. One of the merits of the presented method is that the point cloud data are directly used, rather than a 2.5D interpolated or triangular irregular network (TIN) generation, thereby significantly enhancing the accuracy of the normal vector estimation. Furthermore, the CFSFDP method does not have an initialization problem (the number of clusters is not required). This approach, however, cannot detect line-type traces of discontinuities in an outcrop.

Chen et al. (2020) proposed a four-stage procedure: a normal vector calculation of the point cloud, a modified RANSAC algorithm, delineation of discontinuity boundary by a modified Graham scan algorithm, and the orientation estimation based on discontinuity.

The visual segmentation results for these studies and that of Riquelme et al. (2014) are illustrated in Fig. 13. Some examples of deficiencies are indicated by rectangles and the type of deficiency (EA: empty area; OS: over-segmentation; MS: mis-segmentation; IS: incomplete segmentation; US: under-segmentation). Fig. 13(a) shows highly over-segmented discontinuities compared with other studies in Fig. 13. The over-segmentation areas and the number of data points removed as noise in Fig. 13(c) are fewer compared with Fig. 13(a). Fig. 13(b) and (c) suggest more smooth segmentation results for the discontinuities, which lead to more distinguishable boundaries and the area of the discontinuities. However, this may include shortcomings such as mis-segmentation, incomplete-segmentation, and under-segmentation due to merging two or more planes.

Riquelme et al. (2014) and Chen et al. (2020) previously measured the ground truth orientations of discontinuities for PC2. Riquelme et al. (2014) manually extracted the orientation data (GT1) using the best-fitting plane to each set of points, following the method presented by Fernández (2005) using Polyworks. Chen et al. (2020) manually extracted the orientation data (GT2) using a best-fitting plane to each set of points using the Compass plugin in CloudCompare. The process was as

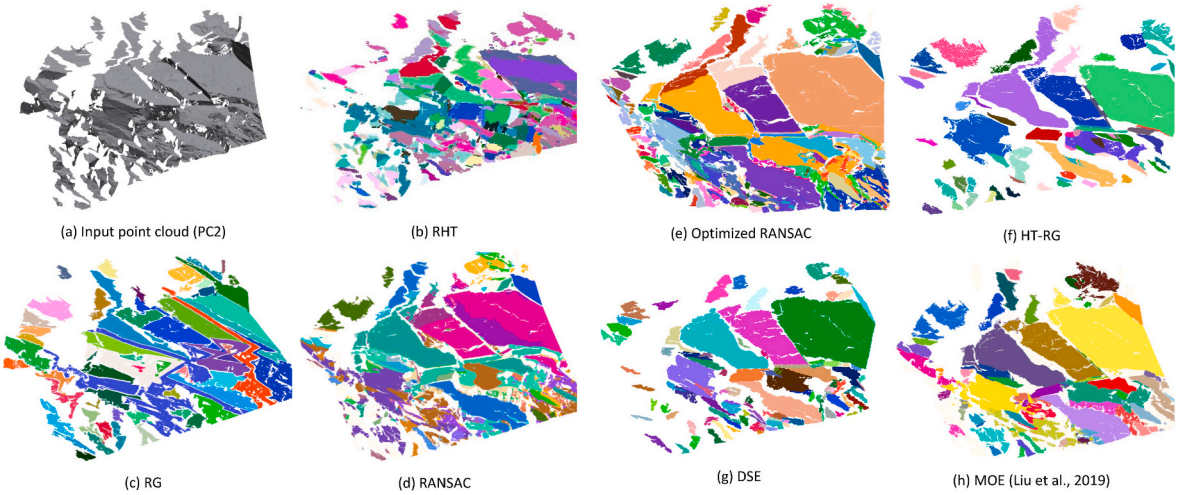

Fig. 11. Qualitative comparison of different methods for PC2 (the raw point cloud was taken from Rockbench (Lato et al., 2013); Execution of segmentation techniques and visualization were conducted by Liu et al. (2019); PCL library for RHT, RG, and RANSAC, and CGAL library for optimized RANSAC were used).

Fig. 12. Comparison of segmentation results for different methods vs. ground truth data for PC1; Raw dataset provided by Lato et al. (2013) and visualization of methods presented by Liu et al. (2019).

follows. The plane tool is activated to create a red circle by clicking on a point in the point cloud; the circle's center is specified. The radius of the circle was controlled through the degree of zooming. Points falling within the circle are used to determine the dip and dip direction with a least-square method for plane fitting. This orientation measurement method can be accurate if the target plane surface is selected using a large circle radius to consider all points on that surface.

A review of the two ground truth datasets (GT1 and GT2) orientations revealed some significant differences with an angle difference of up to 16.5°. This discrepancy prompted an effort to conduct a third manual measurement of the discontinuity orientations from the point cloud. We manually determined the discontinuity orientations using the *Segment* tool in CloudCompare to draw a closed polygon around points falling on a specific discontinuity. Then, the best-fit plane tool in CloudCompare was used to extract the plane's orientation (GT3) (dip and dip direction) from the selected points. This approach is more labor-intensive than the approach used by Chen et al. (2020). However, it can select all points falling on a plane to determine a more accurate and representative discontinuity orientation.

The ground truth measurements and their orientation differences for PC2 are presented in Table 5. The plots displayed in Fig. 14 show the angle differences between the various methods.

It is believed that the ground truth orientations found using CloudCompare give more reliable and reproducible orientation results as all the points of a plane can be extracted. Generally, the GT2 results have a smaller discrepancy with GT3 and are considered better orientation results than GT1. There are three planes, No. 12, 13, and 32, with significant angle differences (14.9°, 10.8°, and 11.7°) when comparing GT3 with GT1. The highest angle discrepancies observed between GT2 and GT1 are for planes No. 32 (16.5°) and 41 (15.2°).

Interestingly, ground truth data deviations exceed those of semi/automatic orientations versus GT3, which may question the validity of the ground truth orientations. Similarly, Drews et al. (2018) introduced two orientation measurement sources as the ground truth data (geological compass and Virtual Reality Geological Studio (VRGS) software) to compare their proposed automatic detection of the discontinuity planes. A mean error (deviation angle) of around 5° (automated vs. compass), 1.8° (automated vs. VRGS software), and 5.2° (compass vs. VRGS software) were reported. The compass measurements were reported to be less precise than the other two digital-based methods, algorithmic and VRGS software, due to curvature, roughness, and accessibility to the complex rock surfaces.

The two main reasons for inconsistent orientations for a target plane seem to be (1) lack of concise specification of plane borders and (2) uneven non-planar sub-surfaces (e.g., single-stepped, multi-stepped, arc-shaped, undulating) relative to the size of the whole plane. It is argued that selecting such planes as ground truth may not lead to reliable and reproducible segmentation and orientation results, and therefore the subsequent comparison could be misleading.

The number assigned for ground truth planes in PC2 (Fig. 15) matched those used in DSE, which is also followed by other studies. This facilitates visualization of results comparison. Examples of problematic discontinuity surfaces with inconsistent orientation measurements in PC2 are described as follows. Plane No. 12 is a comparatively small plane, with a portion of the area like a pothole shown in red. Due to the small area, the segmentation of this plane may partly exclude the red points and the area close to the border. That can lead to a plane fitting with different orientation results. Plane No. 32 has a surface with multiple relatively parallel planes (multi-stepped). Volatile segmentation results can appear depending on the methods and parameter values used, and the resulting plane may include three to five distinct plane segments. Plane No. 33 resembles a single-stepped surface. The segmentation area in blue may split the surface into two distinct plane segments. For plane No. 41, all comparisons of ground truth orientation data in Table 5 show a comparatively high angle difference because this plane is a multi-planar surface, and the resultant segmentation may not yield a single or three-plane segment, as shown in Fig. 16. The boundaries for Plane No. 52 are indefinite and lead to inconsistent interpretation by users who set the boundary for the ground truth. This plane can be split into two (or more) smaller segments, mainly including an arc-

Table 4
Summary of various methods to segment discontinuities from rock surface point clouds (performance metrics: P (precision) |R (recall) |F1 (F1-score)).

Method	Technique	Advantages	Deficiencies	By Yu et al. (2020) for PC1	
				Run time (s)	P| R| F1 (%)
RHT using PCL	Model-fitting	Quite fast	Over-segmentation, Wrong/ inaccurate plane boundaries, Relative high computation time	40	74| 78| 76
RG using PCL	Seed growth and neighboring info	seed points and criteria to grow can be determined	Incorrect planes, over-segmentation, Wrong/ inaccurate plane boundaries, Sensitive to seed growing	12.2	78| 76| 77
RANSAC using PCL	Model-fitting	Robust to noise	Over-segmentation, Spurious planes, Inaccurate plane boundaries, Missing small and low-density surfaces, Relative high computation time	28.4	82| 81| 81
Optimized RANSAC using CGAL	Model-fitting	Fast	Over-segmentation, Inaccurate plane boundaries, Missing small and low-density surfaces,	2.9[a]	85| 84| 85[a]
HT-RG (Leng et al., 2016)	Model-fitting and Region growing	Multi-scale planes can be found	Over-segmentation, Missing small and low-density surfaces, relative high computation time	151.1	91| 86| 88
MOE (Liu et al., 2019)	Gaussian kernel estimation and Neighboring info	Very fast, Preserves the boundaries of planes, Good accuracy	Missing small and low-density surfaces, Large number of parameters to tune	1.1	92| 92| 92
RAN-RG (Hu et al., 2020)	Model-fitting and Region growing	Fast, Preserves the boundaries of planes, Good accuracy	Missing small and low-density surfaces	1.7	91| 92| 91
Supervoxel-RG (Yu et al., 2020)	RANSAC and Region growing	Fast, Preserves the boundaries of planes, Good accuracy	Leaving holes in some planes, over-segmentation	4.1	95| 98| 96

[a] Numeric results of optimized RANSAC using CGAL are taken from Liu et al. (2019).

shaped surface area.

Extra caution is needed when dealing with discontinuities with profiles similar to those shown in Fig. 16 to minimize the deviation from ground truth orientations and produce a more objective plane specification as a reference. It is recommended to compare both precision and recall as the two common performance indexes since the former shows the degree of false positives and the latter does that of false negatives. This provides a more informed perspective of the relationship between the ground truth and prediction results.

For rock mass surfaces that are highly irregular, setting a concrete ground truth segmentation of discontinuity planes in the corresponding point cloud can be challenging and questionable. In such cases with a higher degree of uncertainty, the ground truth should be adjusted considering the geometry, field observation, and engineering judgment to maintain more tangible fact-tested ground truth results.

Segmentation results of discontinuities from a rock surface point cloud may include over-segmentation, under-segmentation, mis-segmentation, or removed surface areas due to sparse density and noise removal steps. The degree of over/under-segmentation can be partially controlled by adjusting the hyperparameter values, depending on the methods used. For instance, increasing the *knn* value in the normal vector estimation can reduce over-segmentation.

The voxel-grid downsampling reduces the effect of uneven discontinuity surfaces and helps control the over-segmentation phenomenon (Daghigh et al., 2021). This downsampling works best when the point cloud density is relatively high compared to the size of the planes intended to be detected. This technique may be used as a pre-processing step (Daghigh et al., 2021) or after the segmentation. However, when used as a pre-processing step, it can more efficiently diminish the unexpected over-segmentation areas shown in Fig. 16. However, a large voxel size causes the curvature of the intersection(s) between planes to be reduced, which increases the likelihood of merging planes in the segmentation results. As a result, it yields under-segmentation and mis-segmentation areas. Therefore, the voxel size should be optimized for each rock surface point cloud considering the size and type of planes required to be extracted.

A collection of studies with technique(s), input data used, and their advantages and deficiencies are summarized in Table 6.

5. Open-source tools to extract discontinuity planes

Commercial and open-source software can be used to extract discontinuities using various methods and techniques. Examples of commercial software include RockScan (Ferrero et al., 2009), Coltop-3D (Jaboyedoff et al., 2009), Split-FX, Maptek PointStudio ("Split-FX Analysis Service," 2021), DiAna (Gigli and Casagli, 2011), Visualization Toolkit (Vöge et al., 2013), ShapeMetrix 3D ("ShapeMetrix 3D," n.d.), and Sirovision (Datamine Software). FACETS (Dewez et al., 2016) is a tool to extract the planar surfaces from 3D point clouds as a plugin in the open-access CloudCompare software ("CloudCompare User Manual," 2021). A MATLAB tool, PlaneDetect (Li et al., 2019), was introduced in 2019, but the source code is not publicly available.

The two open-source tools, CloudCompare and Discontinuity Set Extractor (DSE) (Riquelme et al., 2014), are selected for further discussion because they are publicly available and popular among researchers. The capabilities of CloudCompare to extract discontinuity planes are demonstrated using a point cloud of a dodecahedron and a real rock mass dataset. The methodology used by DS is briefly presented, and its performance is discussed.

5.1. CloudCompare

CloudCompare can be used to analyze point clouds related to earth

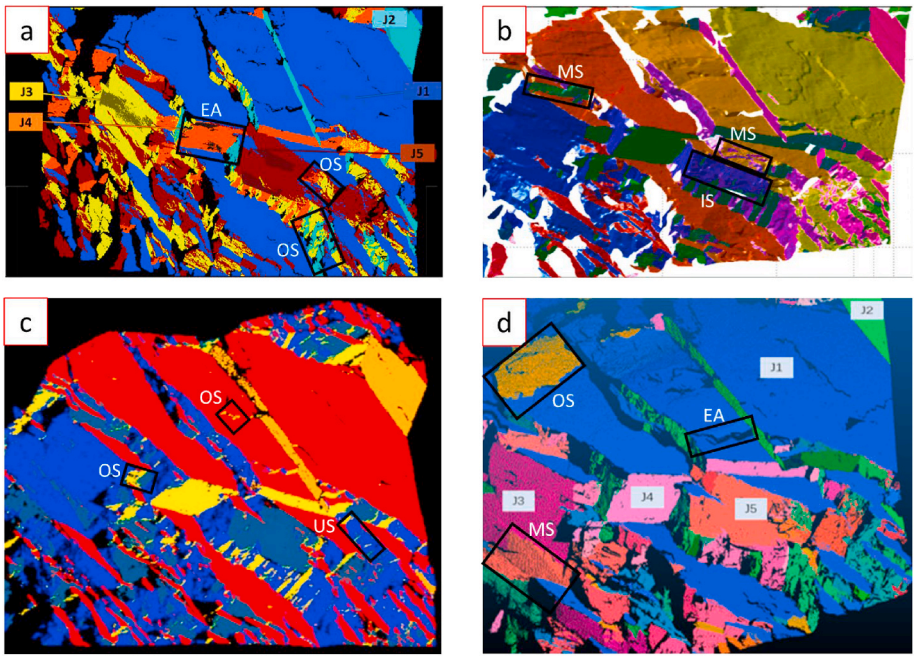

Fig. 13. Segmentation comparison with examples of deficiencies for PC2 (the raw point cloud was provided by (Lato et al., 2013)), (a) Riquelme et al. (2014), (b) Chen et al. (2016), (c) Kong et al. (2020), and (d) Chen et al. (2020).

science and geological structures. CloudCompare is a general 3D data processing software that includes advanced features. It was developed in C++ and is capable of fast processing and handling large 3D datasets. The normal estimation in CloudCompare may not deliver high-quality results for rock mass point clouds because of noisy points, high curvature areas, and non-uniform normal orientations. Thus, automatic detailed extraction of plane surfaces in a complex rock mass point cloud may not be adequately achieved using the current features available in the CloudCompare software.

The following subsections (Normal computation, Delaunay triangulation, Outlier filtering, and RANSAC shape detection) discuss some useful capabilities within CloudCompare.

5.1.1. Normal computation

There are several local surface models in CloudCompare to estimate normal vectors. The first and most common one is Plane, which finds the best-fit plane. This method is robust to noise while not efficient with sharp edges, borders, and corners. The other common method is triangulation, which uses 2D triangles to mesh data points. This method works satisfactorily with sharp edges. However, it is sensitive to noisy data. For the neighbor selection for normal estimation, the octree structure is the default, and all neighboring points within a specified radius are included. The greater the radius, the more points are involved in the computation, and the smoother the result will be. This is at the expense of a higher processing time (CloudCompare User Manual, 2021).

The local surface model only accounts for estimating the direction of the normal. However, the resulting normal orientations (inward or outward) should be adjusted, as they are generally inconsistent. To this end, the Minimum Spanning Tree (MST) algorithm is used to specify the maximum number of neighbors (*knn*) connected to each data point. The greater this number *knn*, the more memory and time are required. Also, the normal vector variation is generally reduced with an increase in *knn*, resulting in a smoother surface in the segmentation stage (Daghigh et al., 2021). Fast Marching (FM) as an alternative to MST can be used. However, FM is not very accurate, and it is strongly recommended to use the MST method (CloudCompare User Manual, 2021).

5.1.2. Delaunay triangulation

In order to mesh the point cloud using triangulation, the point cloud should be projected on a 2D x-y plane or the best fitting plane (least squares). The triangulation is done in 2D space, and the mesh structure is applied to the 3D points. The maximum length parameter for the edges of the triangle can be determined. The normal vector can be calculated for each triangle, and sharp edges are better preserved (CloudCompare User Manual, 2021).

5.1.3. Outlier filtering

Point cloud datasets often include outliers, points that are connected to the majority sampling a surface. These outliers introduce errors in the estimation of normals and curvatures. By applying a statistical outlier removal (SOR) analysis to the neighborhood of each point, those points failing to satisfy a particular criterion are removed. This method is based on the computation of the mean distance of each point to all its neighbors (CloudCompare User Manual, 2021). Assuming a Gaussian distance distribution, all points outside a defined mean and standard deviation are assumed as outliers and removed from the dataset.

A noise filter tool based on the relative or absolute distance of a point to a best-fit plane can be used to filter points. The points selected to find the best-fit plane are defined with a knn value or a sphere radius. This algorithm fits a plane to these points and removes any point found to be too far from the fitted plane. This filter tool works best for point clouds representing planar surfaces. Using a very high kernel radius or very small error threshold should be avoided as this will not preserve sharp edges and corners ("CloudCompare User Manual," 2021). Instead, it is recommended to use a small radius and comparatively high error threshold while the algorithm is run repeatedly. The application of the noise filter on a dodecahedron point cloud dataset is displayed in Fig. 17. As shown in the rectangular area, this filter effectively removes noisy points near the planar surface.

A fixed neighborhood radius (R) is specified along with a relative max error (with respect to the fitted plane) to determine whether a point is filtered.

The RANSAC shape detection algorithm in CloudCompare was designed by Schnabel et al. (2007), and it can be used as a plugin. Based on random sampling, this algorithm automatically detects basic shapes,

Table 5
Different ground truth manual mapping results and orientation differences for PC2 (GT1 by Riquelme et al. (2014), GT2 by Chen et al. (2020), and GT3: present study).

Plane	Ground truth dip direction and dip and their differences					
	Dip direction/Dip (°)			Orientation differences (°)		
	GT1	GT2	GT3	GT3 vs. GT2	GT3 vs. GT1	GT2 vs. GT1
11	249.2/ 40.2	242/ 41	246.1/ 39.1	3.2	2.3	4.8
12	264.2/ 57.0	255/ 50	248.1/ 49.5	5.3	14.8	10.5
13	264.0/ 41.9	248/ 36	249.8/ 35.7	1.1	10.8	11.6
14	252.6/ 36.5	251/ 35	251.8/ 34.7	0.5	1.9	1.8
15	248.7/ 37.0	248/ 37	249.3/ 35.4	1.8	1.6	0.4
16	254.8/ 29.8	249/ 35	250.1/ 35.7	0.9	6.4	6.1
17	249.9/ 35.9	254/ 34	253.4/ 33.3	0.8	3.3	3
21	338.7/ 82.4	342/ 83	339.5/ 83.1	2.5	1.1	3.3
22	347.5/ 79.0	347/ 71	345.7/ 73.2	2.5	6.1	8.0
23	341.0/ 89.5	347/ 86	338.2/ 88.1	9	3.1	6.9
24	353.5/ 76.4	174/ 76	173.7/ 76.7	0.8	0.4	0.6
31	314.1/ 77.2	133/ 81	136.7/ 77.0	5.4	2.5	4.0
32	302.4/ 75.9	137/ 84	131.0/ 84.0	6.0	11.7	16.5
33	330.2/ 83.0	144/ 89	147.2/ 89.1	3.2	6.8	8.6
41	286.1/ 58.9	100/ 73	97.2/ 62.2	11.1	8.4	15.2
42	274.2/ 51.1	91/47	92.5/ 48.6	1.9	2.8	4.8
43	277.2/ 46.4	95/46	97.7/ 48.8	3.4	2.4	1.6
51	305.0/ 77.6	305/ 78	304.4/ 77.9	0.6	0.7	0.4
52	290.2/ 67.0	286/ 70	286.7/ 70.7	1.0	4.9	4.9
Ave.	–	–	–	3.2	4.8	5.9
S.D.	–	–	–	2.9	4.0	5.7

including planes. This method is simple and robust to noise and should be used on a point cloud with consistent normals.

The RANSAC algorithm was demonstrated on a point cloud representing a dodecahedron (Fig. 18) and PC2 (Fig. 19) with changing point density and plane sizes. The dodecahedron point cloud dataset was acquired using a 3D digitizer and provided by Riquelme et al. (2014), and it contains 40414 points, and its bounding box is around 62 × 60 × 32 mm. The RANSAC algorithm generally works best on a point cloud with accurate normals. The optimal values for parameters used in the RANSAC implementation demonstrated in Figs. 18(b), and Fig. 19(b) are presented in Table 7. RANSAC in CloudCompare effectively detects planar surfaces in the simple dodecahedron point cloud by choosing a proper set of values for the parameters. The spurious planes may be detected if a different distance threshold is used (Fig. 18(c)).

For a complex point cloud of a rock mass, running RANSAC multiple times with various combinations of parameters may still not lead to the proper detection of all the planar surfaces. When the size and density of planar faces in a rock mass point cloud are highly variant, spurious planes are likely detected, while some planes are left undetected. Fig. 19 (b) shows the rock mass point cloud for which most planes were detected, including a few spurious planes. Nevertheless, some areas that are shown in yellow rectangles in Fig. 19(a) were undetected. In Fig. 19 (c), some undetected planes shown in Fig. 19(b) are detected, yet the number of spurious planes exceeds ten.

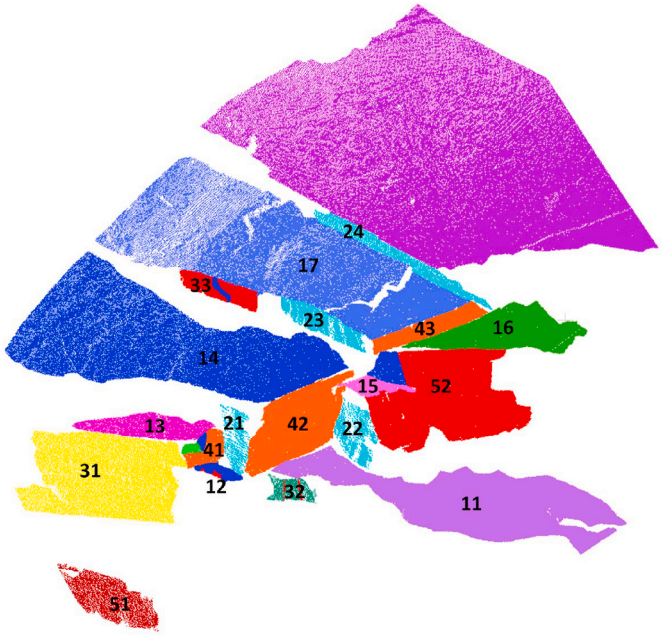

Fig. 15. Ground truth planes displayed in the present work for PC2 with the same numbering scheme used in DSE.

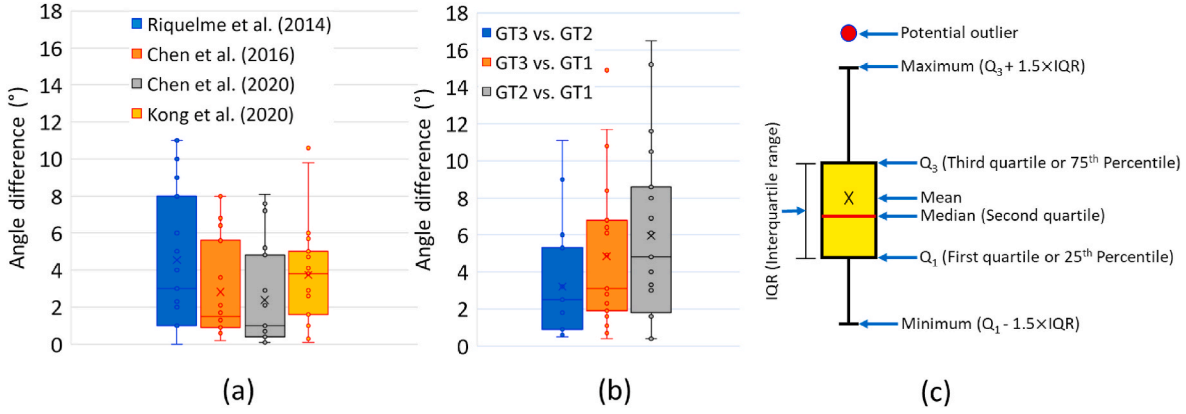

Fig. 14. Comparison of orientation results for PC2. (a) Evaluation of various semi-/automated orientation extraction methods versus our ground truth (GT3), (b) Deviation of ground truth results (GT1: Riquelme et al. (2014); GT2: Chen et al. (2020); GT3: present study), (c) Box plot specifications.

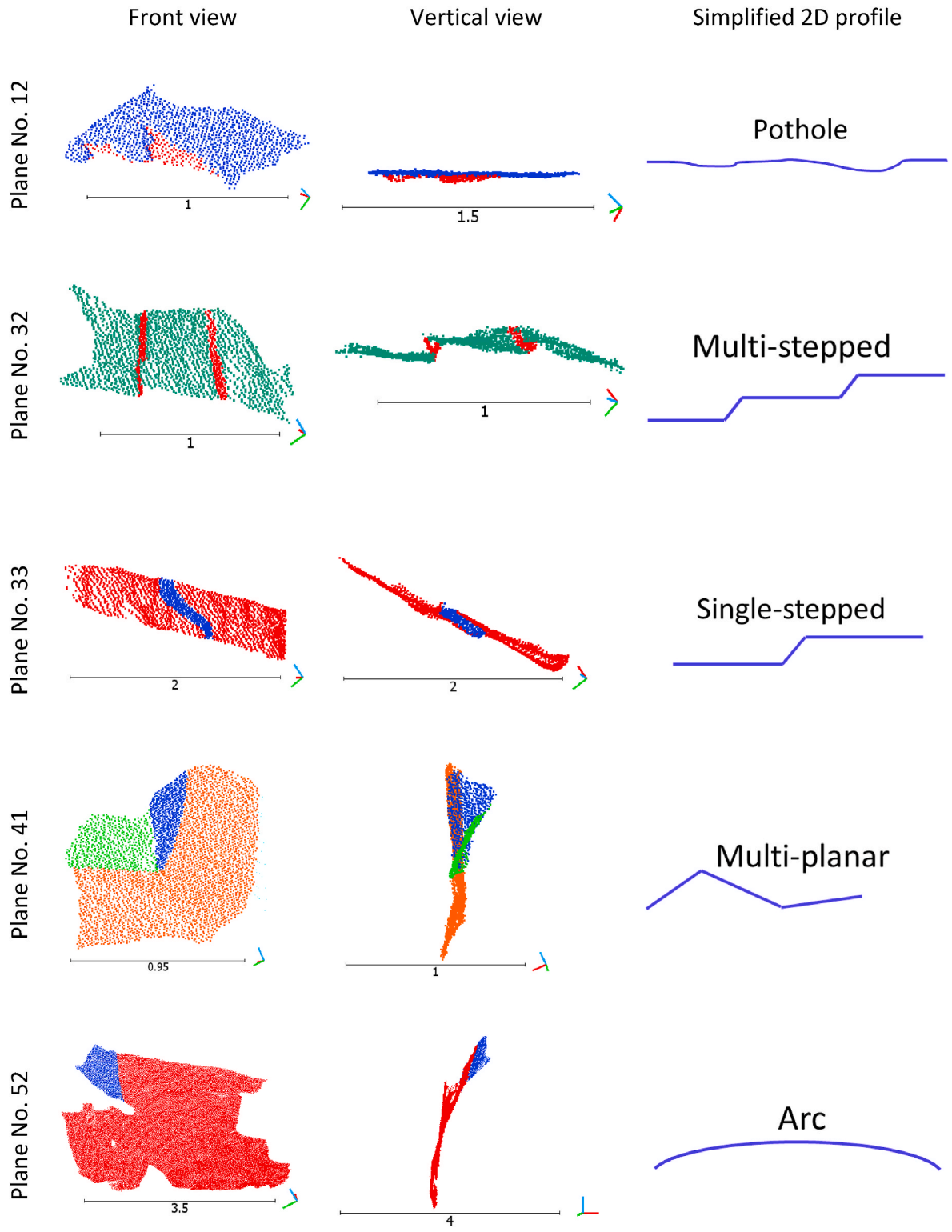

Fig. 16. Discontinuity surfaces in PC2 cause a high discrepancy in orientation results (scale bar unit is in meters).

The RANSAC algorithm in CloudCompare may satisfactorily detect the planes in regular shaped point clouds. However, its implementation on the rock mass point cloud cannot fully detect all correct planes with one set of parameter values. The RANSAC may also detect small planes with sparse density, but it comes at the expense of yielding incorrect planes, which is inefficient. Therefore, implementing just RANSAC, in its current form, on a complex rock mass point cloud may not deliver satisfactory plane detection results.

5.2. *Discontinuity Set Extractor (DSE)*

The DSE is an open-source tool developed in MATLAB (Riquelme et al., 2014) to process 3D point clouds. The tool operates in three main stages (Fig. 20):

1) Local curvature calculation (plane detection) is done using the nearest neighbor search. A fixed number of neighbors is preferred

Table 6
Summary of studies for extraction of discontinuity traces and planes.

Method	Technique	Input	Advantages	Deficiencies
Reid and Harrison (1997)	Edge based	2D image	Relatively simple, Fast	Incomplete and spurious, 2D traces
Gonzalez et al. (2002)	Edge based	2D image	Suitable for limestone	Semi-automatic, Unsatisfactory for carbonatite and granodiorite exposures, 2D traces
Lemy and Hadjigeorgiou (2003)	Edge based	2D image	Relatively simple, Fast	Incomplete and noisy, 2D traces
DSE (Riquelme et al., 2014)	Clustering using DBSCAN and kernel density estimation	3D point cloud	Robust to noise, comparison with the developed ground truth orientations for the point cloud for each plane, Satisfactory accuracy	Semi-automatic, Computationally expensive, over-segmentation, large number of parameters to tune
Chen et al. (2016)	Clustering using an improved K-means and RANSAC	Digital surface model (TIN)	Automatic, Robust to the surface irregularity and roughness, Number of the cluster is set by the Silhouette validity index, Good accuracy	Choosing a proper triangular mesh size can be challenging, Normal vectors are so sensitive to noise due to TIN as input, High computation time due to optimization
Wang et al. (2017)	Region growing	3D point cloud	Automatic,	Not suitable for areas larger than 70 m^2, over-segmentation, computationally expensive for point cloud over 1 million points, inaccurate plane boundaries
Bolkas et al. (2018)	Edge based	3D surface	Relatively simple, Fast	2D traces, noisy, discrete sets of edges
Guo et al. (2018)	Edge based	3D point cloud	3D detection, Automatic, more efficient than manual or semi-automated methods	No distinction between discontinuity trace and other fractures (e.g., blasting)
Ge et al. (2018)	Region growing	3D point cloud	Automatic, use of a modified RG with enhanced run-time efficiency compared with regular RG	Over-segmentation, qualitative segmentation comparison for each plane, and lack of ground truth point cloud
Zhang et al. (2018)	Clustering using mean-shift and Region growing	Digital surface model	Automatic, few key hyperparameters need to be set	Computationally expensive, prone to error due to triangulation than the direct use of 3D coordinates
Guo et al. (2018)	Clustering using FCM	3D point cloud	Automatic, Voxelization to smooth and reduce over-segmentation, number of clusters estimated using FA	Inaccurate plane boundaries, qualitative segmentation comparison for each plane, and lack of ground truth point cloud
Drews et al. (2018)	Region growing	3D point cloud	Automatic, comparison with the two sets of ground truth orientations for the point cloud, Good accuracy	Computationally expensive (high computation for normals), large number of parameters to tune
Zhang et al. (2019)	Edge based	2D image and 3D point cloud	3D, Automatic, Efficient	No distinction between discontinuity trace and other fractures, no detailed detection
Kong et al. (2020)	Clustering using CFSFDP and RANSAC	3D Point cloud	Automatic, Improved normal estimation ar sharp edges using iterative reweighted plane fitting (IRPF), No need to specify the number of clusters, Satisfactory accuracy	High computation time, Lack of line-type discontinuity traces (e.g., perpendicular to the surface rock outcrop)
Chen et al. (2020)	Modified RANSAC	3D Point cloud	Automatic, Good accuracy	Some under- and over-segmentation areas
Singh et al. (2021)	Clustering using K-Medoids and DBSCAN	3D point cloud	Satisfactory accuracy, Ground and vegetation removal, Orientation comparison with other results	Unclear border for ground truth planes

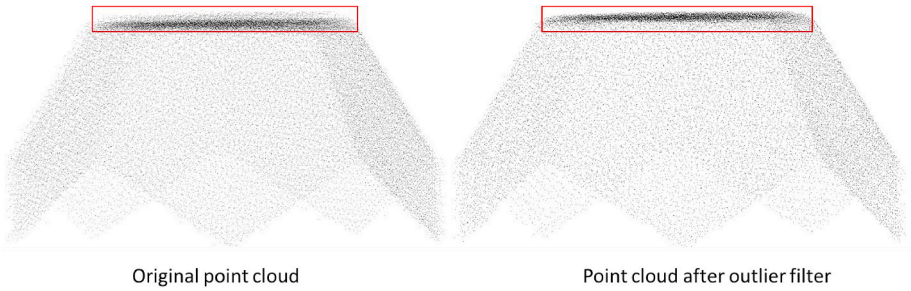

Fig. 17. Noise filter implementation (R = 1 mm and relative max error = 1) (the raw point cloud presented by (Riquelme et al., 2014) and the dataset was accessed at http://www.3d-landslide.com/projects/discontinuity/) RANSAC shape detection.

because errors may arise when using a fixed distance due to changing point density (Lato et al., 2010; Riquelme et al., 2014). Next, a coplanarity test is conducted using PCA by considering a specified threshold. This analysis checks whether the surrounding points fall within the same plane. After all coplanar points are recognized, the normal to the plane is obtained using the eigenvector.

2) Statistical analysis of the planes using stereographic projection.
3) Clustering analysis is performed using DBSCAN, PCA, and a check on the error fitting. Two parameters are required as input, the distance threshold between two points as neighbors, ε, and a minimum neighboring point q (a core point), in that threshold, Min-pts. It was reported that large variations in the point density might cause processing difficulty (Ester et al., 1996; Lato et al., 2010). It was recommended by Ester et al. (1996) to set the Min-pts parameter to 4 and ε by considering the distance of the 4th neighbor for each discontinuity set.

A clustering analysis may detect many small clusters in a point cloud. The user may disregard small clusters and only consider clusters with a sufficient number of points (Riquelme et al., 2014).

The following subsections present parameters setting for the coplanarity, the effects of *knn*, deviation tolerance, and pole dispersion in the

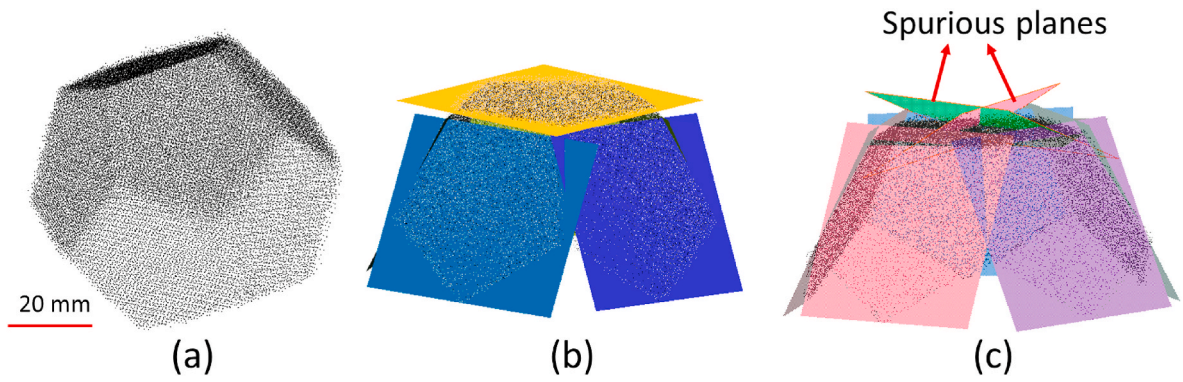

Fig. 18. (a) Raw point cloud data of dodecahedron, (b) RANSAC implementation on the dodecahedron point cloud with six planes detected using parameter values in Table 7, (c) RANSAC implementation on a dodecahedron point cloud (max distance to primitive = 2 mm; two spurious planes detected).

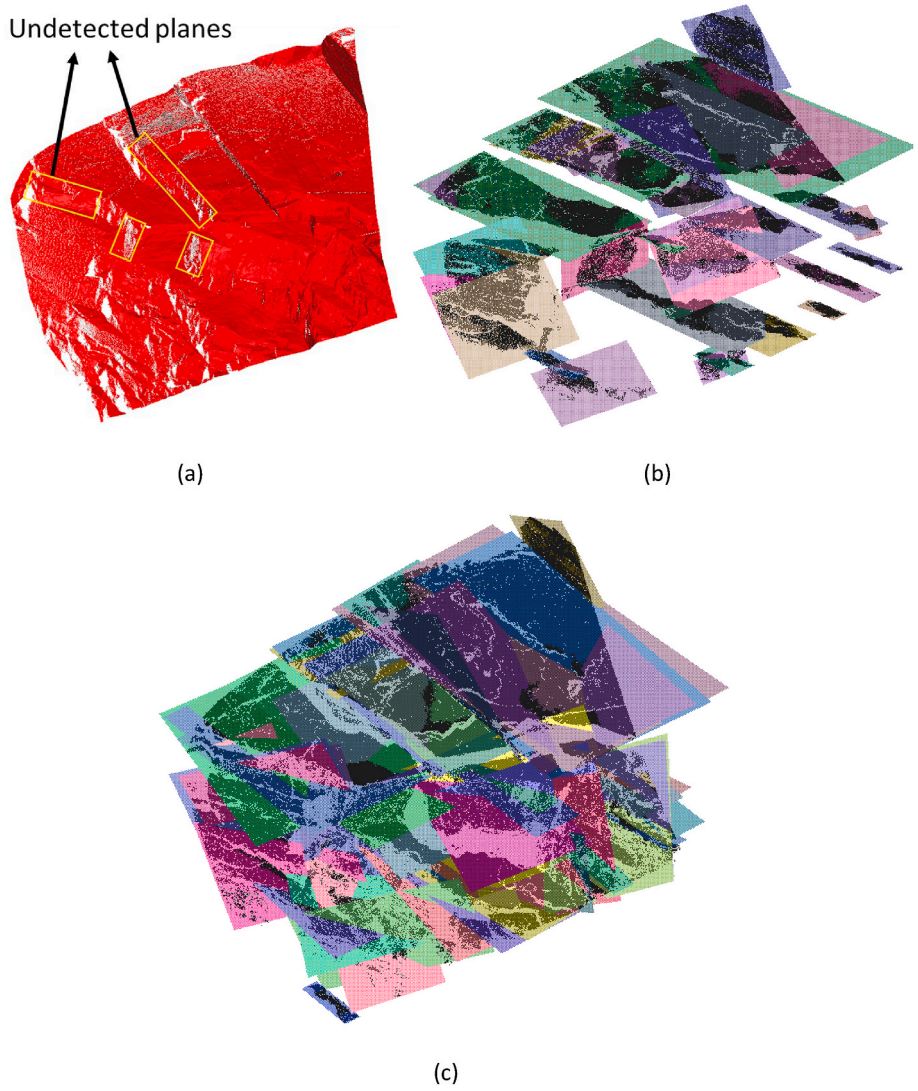

Fig. 19. (a) Raw point cloud data (PC2), (b) RANSAC implementation on the rock mass point cloud with 36 planes detected using parameter values in Table 7, (c) RANSAC implementation on the rock mass point cloud (max distance to primitive = 0.1 m; over ten spurious planes detected).

cluster analysis in the DSE.

5.2.1. Coplanarity, number of neighbors, and deviation tolerance

For coplanarity calibration, the number of neighbors *knn* and the maximum deviation η are the most important parameters to select. The process may start with a variation of *knn* to examine the η_{max}. It is crucial to choose a value such that only noisy data is disregarded rather than valuable data points. If a low value is assigned to *knn*, the value for η is often high, while this correlation diminishes if *knn* increases (Riquelme et al., 2014).

Table 7
Optimal parameters used for the RANSAC shape detection algorithm in CloudCompare for dodecahedron and PC2 datasets.

	Min support points per primitive	Advanced parameters			
		max distance to primitive	sampling resolution	max normal deviation	overlooking probability
dodecahedron	300	0.31 mm	0.620	20°	0.01
PC2	1000	0.02 m	0.1	10°	0.01

Based on sensitivity analysis (Riquelme et al., 2014), selecting a high *knn* and a low η_{max} leads to a better distinction between planar and non-planar features. In their case study, a low number of neighbors (*knn*<15) resulted in outlier points being included in the pole estimation. In contrast, a higher *knn* (*knn*>30) overly smoothed the local curvature. Therefore, a range of 15–30 for *knn* was an optimal tradeoff between accuracy and resolution. As well, the optimal value for η_{max} was around 20%.

5.2.2. Pole dispersion effects in the cluster analysis

The number of neighbors, *knn*, impacts the way that poles are dispersed in the stereo-plot. An increase in *knn* results in a higher concentration of normal vectors around the mean. This suggests that higher precision is attained with more neighbor points. A summary of the optimal parameters found when processing the dodecahedron point cloud is presented in Table 8. Note that γ_2 is the maximum threshold for the associated normal vector and the assigned principal plane normal vector.

After a comprehensive sensitivity analysis (Riquelme et al., 2014), the number of neighbors was considered of prime importance in determining planar features and non-planar ones like edges and vertices. Meanwhile, the coplanarity test was found as the most computationally expensive procedure in their method, increasing the run time as larger *knn* values are used.

Riquelme et al. (2014, 2015) improved the capability of DSE by adding the ability to estimate the discontinuity normal spacing and persistence.

DSE workflow can handle noisy point cloud data. One advantage of this method is the direct use of 3D data points without utilizing a 2.5D interpolated mesh surface. It also recognizes some areas with curvature on a discontinuity plane as noise points and removes them, and this leads to areas where planes are not extracted. DSE is not a fully automatic approach and tends to yield over-segmented plane clustering results.

6. Conclusions

The evolution in the 3D point cloud data analysis of rock faces has improved the extraction of rock discontinuities. The number of publications on the 3D automatic extraction of discontinuity planes has accelerated over the past decade. This paper reviewed various methods to segment and extract discontinuity plane surfaces from 3D point cloud data. The advantages and limitations of each method, along with their improved versions, were discussed. Generally, machine-learning approaches (unsupervised clustering-based methods) may yield better performance for large complex datasets than surface fitting methods.

Detailed comparative results in the literature were critically discussed qualitatively and quantitatively. The quantitative results evaluate segmentation performance and orientation of discontinuity planes compared to ground truth data. The deviation of ground truth orientations is analyzed, and the reasons and the potential solutions for deriving more reliable ground truth orientation data from a rock face point cloud are discussed.

A comparison of results suggests that hybrid methods, when appropriately deployed, can enhance the segmentation quality and orientation estimation of discontinuities compared with conventional methods used individually. This is because using different techniques for different stages in the hybrid methods offers the advantage of better segmentation results with less over-/under-segmentation of discontinuity planes compared with conventional methods when applied indiscriminately across all stages.

6.1. Recommendations and future directions

Future research should be directed toward more accurate normal vector calculation and better preservation of edges and boundaries of planar surfaces in a rock mass point cloud. Section 3.6 of this article discusses interesting methodologies that have not yet been implemented on rock mass point cloud data but hold promise for addressing edge preservation in rock mass point clouds.

To handle the noise for processing the rock surface point clouds, pre-

Table 8
Summary of the optimal values suggested by Riquelme et al. (2014) for parameters in each stage in DSE.

Stage No.	Parameter(s)		
Stage 1	*knn=30*	$\eta_{max} = 20\%$	–
Stage 2	$\gamma_1 = 20°$	$n_P = 20$	$\gamma_2 = 30°$
Stage 2	$ppc = 50$	–	–

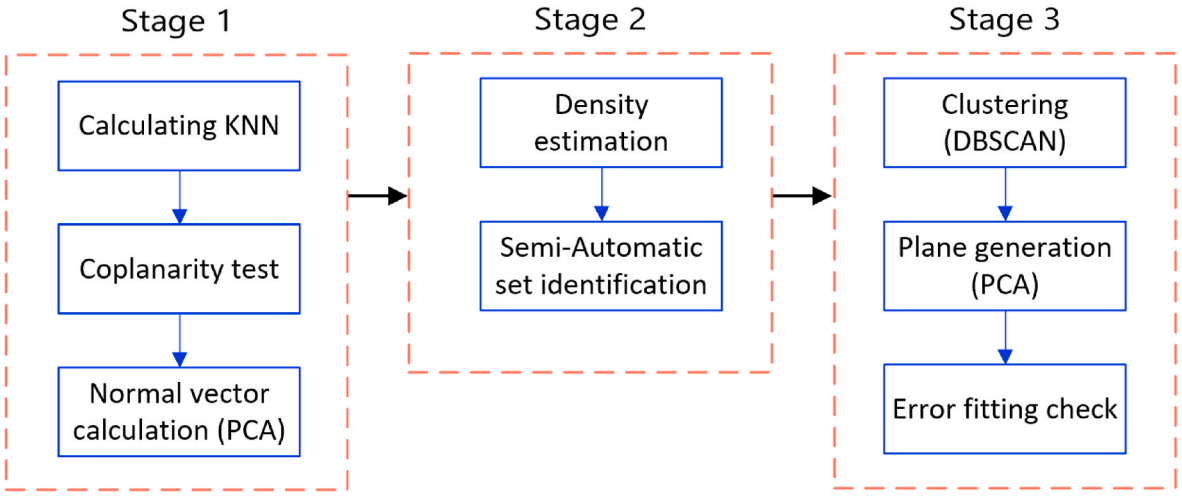

Fig. 20. Summary of procedures used in DSE (Riquelme et al., 2014).

processing and post-processing steps, including downsampling and voxelization, can be helpful and efficient approaches for large point clouds.

Most 3D point cloud processing methods ignore the color information and rely solely on geometry-based methods to extract discontinuity planes. Further improvements to 3D point cloud analysis methods to extract discontinuities should incorporate both geometry and spectral information. Workflows to extract geometrically planar surfaces through processing XYZ coordinates may find planar surfaces that are not discontinuities in rock, such as a uniform soil slope (talus) on a rock face or a rock fracture created by blasting. It is, therefore, essential to have high-quality, dense point clouds with coordinates and texture information (RGB color). For instance, planar-like surfaces that are not discontinuities may be detected by investigating how their roughness pattern and color differ from rock discontinuities.

Publicly available point cloud datasets provide a solid platform for testing, evaluating, and comparing the performance of various algorithms. However, very few datasets are available in online repositories. Researchers should contribute new high-quality point clouds to public repositories to expand the variety of geological features (such as faults, bedding planes, and joints) captured in the available datasets. Most available rock mass point clouds originate from LiDAR surveys, and it would be helpful to have more datasets acquired with photogrammetry. The most efficient and stable approach for hosting a repository of datasets is a professional society website or a public repository such as GitHub that can be continuously monitored, maintained, and updated. It is strongly recommended that the point cloud data from open repositories be used when researchers present a new workflow and demonstrate the capabilities of their method. This facilitates a meaningful comparison of results and builds an enhanced understanding of the strengths and the research gaps, which can significantly propel the advances in rock engineering-related studies.

Declaration of competing interest

The authors declare that they have no known competing financial interests or personal relationships that could have appeared to influence the work reported in this paper.

Data availability

Two rock surface point clouds used in the paper are provided in the Appendix A.

Acknowledgments

The authors wish to thank the insightful comments and valuable feedback they received from the associate editor and the anonymous reviewers, which led to the enrichment of this paper.

Appendix A. Supplementary data

Supplementary data to this article can be found online at https://doi.org/10.1016/j.cageo.2022.105241.

References

Abellán, A., Oppikofer, T., Jaboyedoff, M., Rosser, N.J., Lim, M., Lato, M.J., 2014. Terrestrial laser scanning of rock slope instabilities. Earth Surf. Process. Landforms 39, 80–97. https://doi.org/10.1002/esp.3493.

Adam, A., Chatzilari, E., Nikolopoulos, S., Kompatsiaris, I., 2018. H-RANSAC: a hybrid point cloud segmentation combining 2D and 3D data. In: ISPRS Annals of the Photogrammetry, Remote Sensing and Spatial Information Sciences, pp. 1–8. https://doi.org/10.5194/isprs-annals-IV-2-1-2018.

Aljumaily, H., Laefer, D.F., Cuadra, D., 2017. Urban point cloud mining based on density clustering and MapReduce. J. Comput. Civ. Eng. 31 https://doi.org/10.1061/(ASCE)CP.1943-5487.0000674.

Ankerst, M., Breunig, M.M., Kriegel, H.P., Sander, J., 1999. OPTICS: ordering points to identify the clustering structure. SIGMOD Rec. (ACM Spec. Interes. Gr. Manag. Data) 28, 49–60. https://doi.org/10.1145/304181.304187.

Askari, S., 2021. Fuzzy C-Means clustering algorithm for data with unequal cluster sizes and contaminated with noise and outliers: review and development. Expert Syst. Appl. 165, 113856 https://doi.org/10.1016/j.eswa.2020.113856.

Awwad, T.M., Zhu, Q., Du, Z., Zhang, Y., 2010. An improved segmentation approach for planar surfaces from unstructured 3D point clouds. Photogramm. Rec. 25, 5–23. https://doi.org/10.1111/j.1477-9730.2009.00564.x.

Ballast, D.K., 2007. Handbook of Construction Tolerances. John Wiley & Sons, Hoboken, NJ, USA.

Barath, D., Matas, J., 2018. Graph-cut RANSAC. In: Proceedings of the IEEE Computer Society Conference on Computer Vision and Pattern Recognition, pp. 6733–6741. https://doi.org/10.1109/CVPR.2018.00704.

Battulwar, R., Zare-Naghadehi, M., Emami, E., Sattarvand, J., 2021. A state-of-the-art review of automated extraction of rock mass discontinuity characteristics using three-dimensional surface models. J. Rock Mech. Geotech. Eng. 13, 920–936. https://doi.org/10.1016/J.JRMGE.2021.01.008.

Bauer, J., Karner, K., Schindler, K., Klaus, A., Zach, C., 2003. Segmentation of building models from dense 3D point-clouds. Proc. ÖAGM Laxenburg 253–258.

Bazazian, D., Casas, J.R., Ruiz-Hidalgo, J., 2015. Fast and robust edge extraction in unorganized point clouds. In: 2015 International Conference on Digital Image Computing: Techniques and Applications, DICTA 2015. Institute of Electrical and Electronics Engineers Inc. https://doi.org/10.1109/DICTA.2015.7371262.

Belton, D., Lichti, D., 2006. Classification and segmentation of terrestrial laser scanner point clouds using local variance information. ISPRS Comm. V Symp. 'Image Eng. Vis. Metrol. 5, 44–49.

Bolkas, D., 2019. Assessment of GCP number and separation distance for small UAS surveys with and without GNSS-PPK positioning. J. Survey Eng. 145, 04019007 https://doi.org/10.1061/(asce)su.1943-5428.0000283.

Bolkas, D., Vazaios, I., Peidou, A., Vlachopoulos, N., 2018. Detection of rock discontinuity traces using terrestrial LiDAR data and Space-Frequency transforms. Geotech. Geol. Eng. 36, 1745–1765. https://doi.org/10.1007/s10706-017-0430-6.

Borrmann, D., Elseberg, J., Lingemann, K., Nüchter, A., 2011. The 3D Hough Transform for plane detection in point clouds: a review and a new accumulator design. 3D Res. 2, 1–13. https://doi.org/10.1007/3DRes.02(2011)3.

Bosché, F., Biotteau, B., 2015. Terrestrial laser scanning and continuous wavelet transform for controlling surface flatness in construction - a first investigation. Adv. Eng. Inf. 29, 591–601. https://doi.org/10.1016/j.aei.2015.05.002.

Boulaassal, H., Landes, T., Grussenmeyer, P., Tarsha-Kurdi, F., 2007. Automatic segmentation of building facades using Terrestrial Laser Data. Int. Arch. Photogram. Rem. Sens. Spatial Inf. Sci. 36, W52.

Bremer, M., Wichmann, V., Rutzinger, M., 2013. Eigenvalue and graph-based object extraction from mobile laser scanning point clouds. In: ISPRS Annals of the Photogrammetry, Remote Sensing and Spatial Information Sciences, pp. 55–60. https://doi.org/10.5194/isprsannals-II-5-W2-55-2013.

Campello, R.J.G.B., Moulavi, D., Sander, J., 2013. Density-based clustering based on hierarchical density estimates. In: Lecture Notes in Computer Science (Including Subseries Lecture Notes in Artificial Intelligence and Lecture Notes in Bioinformatics). Springer, Berlin, Heidelberg, pp. 160–172. https://doi.org/10.1007/978-3-642-37456-2_14.

Castillo, E., Liang, J., Zhao, H., 2013. Point cloud segmentation and denoising via constrained nonlinear least squares normal estimates. In: Mathematics and Visualization. Springer Heidelberg, pp. 283–299. https://doi.org/10.1007/978-3-642-34141-0_13.

Chandler, J., 1999. Effective application of automated digital photogrammetry for geomorphological research. Earth Surf. Process. Landforms 24, 51–63. https://doi.org/10.1002/(SICI)1096-9837(199901)24:1<51::AID-ESP948>3.0.CO;2-H.

Chen, D., Zhang, L., Mathiopoulos, P.T., Huang, X., 2014. A methodology for automated segmentation and reconstruction of urban 3-D buildings from ALS point clouds. IEEE J. Sel. Top. Appl. Earth Obs. Rem. Sens. 7, 4199–4217. https://doi.org/10.1109/JSTARS.2014.2349003.

Chen, R.F., Lin, C.W., Chen, Y.H., He, T.C., Fei, L.Y., 2015. Detecting and characterizing active thrust fault and deep-seated landslides in dense forest areas of southern Taiwan using airborne LiDAR DEM. Rem. Sens. 7, 15443–15466. https://doi.org/10.3390/rs71115443.

Chen, J., Zhu, H., Li, X., 2016. Automatic extraction of discontinuity orientation from rock mass surface 3D point cloud. Comput. Geosci. 95, 18–31. https://doi.org/10.1016/j.cageo.2016.06.015.

Chen, N., Cai, X., Li, S., Zhang, X., Jiang, Q., 2020. Automatic extraction of rock mass discontinuity based on 3d laser scanning. Q. J. Eng. Geol. Hydrogeol. 54 https://doi.org/10.1144/qjegh2020-054.

Choi, S., Kim, T., Yu, W., 2009. Performance evaluation of RANSAC family. In: British Machine Vision Conference, BMVC 2009 - Proceedings. https://doi.org/10.5244/C.23.81.

Colesanti, C., Wasowski, J., 2006. Investigating landslides with space-borne synthetic aperture radar (SAR) interferometry. Eng. Geol. 88, 173–199. https://doi.org/10.1016/j.enggeo.2006.09.013.

Comaniciu, D., Meer, P., 2002. Mean shift: a robust approach toward feature space analysis. IEEE Trans. Pattern Anal. Mach. Intell. 24, 603–619. https://doi.org/10.1109/34.1000236.

Daghigh, H., Tannant, D.D., Jaberipour, M., 2021. Discontinuity plane extraction from a rock mass point cloud using unsupervised machine learning. In: International Geoscience and Remote Sensing Symposium (IGARSS). Institute of Electrical and Electronics Engineers Inc., pp. 6151–6154. https://doi.org/10.1109/IGARSS47720.2021.9553816

Datamine Software. https://www.dataminesoftware.com/. (Accessed 15 April 2022).
de Oliveira, L.F.R., Lassiter, H.A., Wilkinson, B., Whitley, T., Ifju, P., Logan, S.R., Peter, G.F., Vogel, J.G., Martin, T.A., 2021. Moving to automated tree inventory: comparison of uas-derived lidar and photogrammetric data with manual ground estimates. Rem. Sens. 13, 1–16. https://doi.org/10.3390/rs13010072.
Deibe, D., Amor, M., Doallo, R., 2020. Big data geospatial processing for massive aerial LiDAR datasets. Rem. Sens. 12, 719. https://doi.org/10.3390/rs12040719.
Dewez, T.J.B., Girardeau-Montaut, D., Allanic, C., Rohmer, J., 2016. Facets : a Cloudcompare plugin to extract geological planes from unstructured 3D point clouds. ISPRS - Int. Arch. Photogramm. Remote Sens. Spat. Inf. Sci. XLI-B5 799–804. https://doi.org/10.5194/isprs-archives-xli-b5-799-2016 di Traglia.
Dong, Z., Yang, B., Hu, P., Scherer, S., 2018. An efficient global energy optimization approach for robust 3D plane segmentation of point clouds. ISPRS J. Photogrammetry Remote Sens. 137, 112–133. https://doi.org/10.1016/j.isprsjprs.2018.01.013.
Drews, T., Miernik, G., Anders, K., Höfle, B., Profe, J., Emmerich, A., Bechstädt, T., 2018. Validation of fracture data recognition in rock masses by automated plane detection in 3D point clouds. Int. J. Rock Mech. Min. Sci. 109, 19–31. https://doi.org/10.1016/j.ijrmms.2018.06.023.
Dube, D., Zell, A., 2011. Real-time plane extraction from depth images with the Randomized Hough Transform. In: Proceedings of the IEEE International Conference on Computer Vision, pp. 1084–1091. https://doi.org/10.1109/ICCVW.2011.6130371.
Duda, R.O., Hart, P.E., 1972. Use of the hough transformation to detect lines and curves in pictures. Commun. ACM 15, 11–15. https://doi.org/10.1145/361237.361242.
Eltner, A., Kaiser, A., Castillo, C., Rock, G., Neugirg, F., Abellán, A., 2016. Image-based surface reconstruction in geomorphometry-merits, limits and developments. Earth Surf. Dyn. 4, 359–389. https://doi.org/10.5194/esurf-4-359-2016.
Ester, M., Kriegel, H.-P., Sander, J., Xu, X., 1996. A density-based algorithm for discovering clusters in large spatial databases with noise. In: Proceedings of the 2nd International Conference on Knowledge Discovery and Data Mining, pp. 226–231.
Fernández, O., 2005. Obtaining a best fitting plane through 3D georeferenced data. J. Struct. Geol. 27, 855–858. https://doi.org/10.1016/j.jsg.2004.12.004.
Ferrero, A.M., Forlani, G., Roncella, R., Voyat, H.I., 2009. Advanced geostructural survey methods applied to rock mass characterization. Rock Mech. Rock Eng. 42, 631–665. https://doi.org/10.1007/s00603-008-0010-4.
Filin, S., 2001. Surface clustering from airborne laser scanning data. Int. Arch. Photogram. Rem. Sens. Spatial Inf. Sci. 34, 119–124.
Filin, S., Pfeifer, N., 2006. Segmentation of airborne laser scanning data using a slope adaptive neighborhood. ISPRS J. Photogrammetry Remote Sens. 60, 71–80. https://doi.org/10.1016/j.isprsjprs.2005.10.005.
Fischler, M.A., Bolles, R.C., 1981. Random sample consensus: a paradigm for model fitting with applications to image analysis and automated cartography. Commun. ACM 24, 381–395. https://doi.org/10.1145/358669.358692.
Fornaciai, A., Bisson, M., Landi, P., Mazzarini, F., Maria, T.P., 2010. A Lidar survey of stromboli volcano (Italy): digital elevation model-based geomorphology and intensity analysis. Int. J. Rem. Sens. 31, 3177–3194. https://doi.org/10.1080/01431160903154416.
Fragoso, V., Sen, P., Rodriguez, S., Turk, M., 2013. EVSAC: accelerating hypotheses generation by modeling matching scores with extreme value theory. In: Proceedings of the IEEE International Conference on Computer Vision. Institute of Electrical and Electronics Engineers Inc., pp. 2472–2479. https://doi.org/10.1109/ICCV.2013.307
Franklin, J.A., Maerz, N.H., Bennett, C.P., 1988. Rock mass characterization using photoanalysis. Int. J. Min. Geol. Eng. 6, 97–112. https://doi.org/10.1007/BF00880801.
Fränti, P., Sieranoja, S., 2019. How much can k-means be improved by using better initialization and repeats? Pattern Recogn. 93, 95–112. https://doi.org/10.1016/j.patcog.2019.04.014.
Furukawa, Y., Ponce, J., 2010. Accurate, dense, and robust multiview stereopsis. IEEE Trans. Pattern Anal. Mach. Intell. 32, 1362–1376. https://doi.org/10.1109/TPAMI.2009.161.
Ge, Y., Tang, H., Xia, D., Wang, L., Zhao, B., Teaway, J.W., Chen, H., Zhou, T., 2018. Automated measurements of discontinuity geometric properties from a 3D-point cloud based on a modified region growing algorithm. Eng. Geol. 242, 44–54. https://doi.org/10.1016/j.enggeo.2018.05.007.
Gélard, W., Devy, M., Herbulot, A., Burger, P., 2017. Model-based segmentation of 3D point clouds for phenotyping sunflower plants. In: VISIGRAPP 2017 - Proceedings of the 12th International Joint Conference on Computer Vision, Imaging and Computer Graphics Theory and Applications. SciTePress, pp. 459–467. https://doi.org/10.5220/0006126404590467.
Gigli, G., Casagli, N., 2011. Semi-automatic extraction of rock mass structural data from high resolution LIDAR point clouds. Int. J. Rock Mech. Min. Sci. 48, 187–198. https://doi.org/10.1016/j.ijrmms.2010.11.009.
Gonzalez, R.C., Woods, R.E., Richard, E., 2002. Digital Image Processing. Prentice Hall.
Gorte, B., 2002. Segmentation of TIN-structured surface models. In: Symposium A Quarterly Journal in Modern Foreign Literatures, pp. 465–469.
Grilli, E., Menna, F., Remondino, F., 2017. A review of point clouds segmentation and classification algorithms. In: International Archives of the Photogrammetry, Remote Sensing and Spatial Information Sciences - ISPRS Archives, pp. 339–344. https://doi.org/10.5194/isprs-archives-XLII-2-W3-339-2017.
Guan, H., Li, J., Cao, S., Yu, Y., 2016. Use of mobile LiDAR in road information inventory: a review. Int. J. Image Data Fusion 7, 219–242. https://doi.org/10.1080/19479832.2016.1188860.
Gumhold, S., Wang, X., Macleod, R., 2001. Feature extraction from point clouds CR categories. In: Proceedings of the 10 Th International Meshing Roundtable, pp. 293–305.
Guo, J., Liu, S., Zhang, P., Wu, L., Zhou, W., Yu, Y., 2017. Towards semi-automatic rock mass discontinuity orientation and set analysis from 3D point clouds. Comput. Geosci. 103, 164–172. https://doi.org/10.1016/j.cageo.2017.03.017.
Guo, J., Wu, L., Zhang, M., Liu, S., Sun, X., 2018. Towards automatic discontinuity trace extraction from rock mass point cloud without triangulation. Int. J. Rock Mech. Min. Sci. 112, 226–237. https://doi.org/10.1016/j.ijrmms.2018.10.023.
Guo, J., Liu, Y., Wu, L., Liu, S., Yang, T., Zhu, W., Zhang, Z., 2019. A geometry- and texture-based automatic discontinuity trace extraction method for rock mass point cloud. Int. J. Rock Mech. Min. Sci. 124, 104132 https://doi.org/10.1016/j.ijrmms.2019.104132.
Hähnel, D., Burgard, W., Thurn, S., 2003. Learning compact 3D models of indoor and outdoor environments with a mobile robot. In: Robotics and Autonomous Systems, pp. 15–27. https://doi.org/10.1016/S0921-8890(03)00007-1.
Hancock, S., Disney, M., Muller, J.P., Lewis, P., Foster, M., 2011. A threshold insensitive method for locating the forest canopy top with waveform lidar. Remote Sens. Environ. 115, 3286–3297. https://doi.org/10.1016/j.rse.2011.07.012.
Hancock, S., Armston, J., Li, Z., Gaulton, R., Lewis, P., Disney, M., Mark Danson, F., Strahler, A., Schaaf, C., Anderson, K., Gaston, K.J., 2015. Waveform lidar over vegetation: an evaluation of inversion methods for estimating return energy. Remote Sens. Environ. 164, 208–224. https://doi.org/10.1016/j.rse.2015.04.013.
Herrera, G., Tomás, R., Vicente, F., Lopez-Sanchez, J.M., Mallorquí, J.J., Mulas, J., 2010. Mapping ground movements in open pit mining areas using differential SAR interferometry. Int. J. Rock Mech. Min. Sci. 47, 1114–1125. https://doi.org/10.1016/j.ijrmms.2010.07.006.
Hirschmüller, H., 2005. Accurate and efficient stereo processing by semi-global matching and mutual information. In: Proceedings - 2005 IEEE Computer Society Conference on Computer Vision and Pattern Recognition, CVPR 2005. IEEE Computer Society, pp. 807–814. https://doi.org/10.1109/CVPR.2005.56.
Hirschmüller, H., 2008. Stereo processing by semiglobal matching and mutual information. IEEE Trans. Pattern Anal. Mach. Intell. 30, 328–341. https://doi.org/10.1109/TPAMI.2007.1166.
Hirschmüller, H., Scharstein, D., 2007. Evaluation of cost functions for stereo matching. In: Proceedings of the IEEE Computer Society Conference on Computer Vision and Pattern Recognition. https://doi.org/10.1109/CVPR.2007.383248.
Hoppe, H., DeRose, T., Duchamp, T., McDonald, J., Stuetzle, W., 1992. Surface reconstruction from unorganized points. Comput. Graph. 26, 71–78. https://doi.org/10.1145/142920.134011.
Hough, P., 1960. Method and Means for Recognizing Complex Patterns.
Hu, L., Xiao, J., Wang, Y., 2020. Efficient and automatic plane detection approach for 3-D rock mass point clouds. Multimed. Tool. Appl. 79, 839–864. https://doi.org/10.1007/s11042-019-08189-6.
Hubert, M., Rousseeuw, P.J., Verdonck, T., 2012. A deterministic algorithm for robust location and scatter. J. Comput. Graph Stat. 21, 618–637. https://doi.org/10.1080/10618600.2012.672100.
Illingworth, J., Kittler, J., 1988. A survey of the hough transform. Comput. Vis. Graph Image Process 44, 87–116. https://doi.org/10.1016/S0734-189X(88)80033-1.
Jaboyedoff, M., Couture, R., Locat, P., 2009. Structural analysis of Turtle Mountain (Alberta) using digital elevation model: toward a progressive failure. Geomorphology 103, 5–16. https://doi.org/10.1016/j.geomorph.2008.04.012.
Jaboyedoff, M., Oppikofer, T., Abellán, A., Derron, M.H., Loye, A., Metzger, R., Pedrazzini, A., 2012a. Use of LIDAR in landslide investigations: a review. Nat. Hazards 61, 5–28. https://doi.org/10.1007/s11069-010-9634-2.
Jaboyedoff, M., Oppikofer, T., Abellán, A., Derron, M.H., Loye, A., Metzger, R., Pedrazzini, A., 2012b. Use of LIDAR in landslide investigations: a review. Nat. Hazards. https://doi.org/10.1007/s11069-010-9634-2.
Javadnejad, F., Slocum, R.K., Gillins, D.T., Olsen, M.J., Parrish, C.E., 2021. Dense point cloud quality factor as proxy for accuracy assessment of image-based 3D reconstruction. J. Survey Eng. 147, 04020021 https://doi.org/10.1061/(asce)su.1943-5428.0000333.
Jiang, X.Y., Meier, U., Bunke, H., 1996. Fast range image segmentation using high-level segmentation primitives. In: IEEE Workshop on Applications of Computer Vision - Proceedings. IEEE, pp. 83–88. https://doi.org/10.1109/acv.1996.572006.
Jones, L., Hobbs, P., 2021. The application of terrestrial LiDAR for geohazard mapping, monitoring and modelling in the British geological survey. Rem. Sens. 13, 395. https://doi.org/10.3390/rs13030395.
Kaiser, A., Ybanez Zepeda, J.A., Boubekeur, T., 2019. A survey of simple geometric primitives detection methods for captured 3D data. Comput. Graph. Forum 38, 167–196. https://doi.org/10.1111/cgf.13451.
Kälviäinen, H., Hirvonen, P., Xu, L., Oja, E., 1995. Probabilistic and non-probabilistic Hough transforms: overview and comparisons. Image Vis Comput. 13, 239–252. https://doi.org/10.1016/0262-8856(95)99713-B.
Khaloo, A., Lattanzi, D., 2017. Robust normal estimation and region growing segmentation of infrastructure 3D point cloud models. Adv. Eng. Inf. 34, 1–16. https://doi.org/10.1016/j.aei.2017.07.002.
Kim, C., Habib, A., Mrstik, P., 2007. New approach for planar patch segmentation using airborne laser data. In: American Society for Photogrammetry and Remote Sensing - ASPRS Annual Conference 2007: Identifying Geospatial Solutions, pp. 368–378.
Kim, C., Habib, A., Pyeon, M., Kwon, G.R., Jung, J., Heo, J., 2016. Segmentation of planar surfaces from laser scanning data using the magnitude of normal position vector for adaptive neighborhoods. Sensors (Switzerland) 16, 140. https://doi.org/10.3390/s16020140.
Kiryati, N., Eldar, Y., Bruckstein, A.M., 1991. A probabilistic Hough transform. Pattern Recogn. 24, 303–316. https://doi.org/10.1016/0031-3203(91)90073-E.
Kong, D., Xu, L., Li, X., Li, S., 2014. K-plane-based classification of airborne LiDAR data for accurate building roof measurement. IEEE Trans. Instrum. Meas. 63, 1200–1214. https://doi.org/10.1109/TIM.2013.2292310.

Kong, D., Wu, F., Saroglou, C., 2020. Automatic identification and characterization of discontinuities in rock masses from 3D point clouds. Eng. Geol. 265, 105442 https://doi.org/10.1016/j.enggeo.2019.105442.
Kuçak, R.A., Özdemir, E., Erol, S., 2017. The segmentation of point clouds with K-means and ann (artifical neural network). In: International Archives of the Photogrammetry, Remote Sensing and Spatial Information Sciences - ISPRS Archives, pp. 595–598. https://doi.org/10.5194/isprs-archives-XLII-1-W1-595-2017.
Kulatilake, P.H.S.W., 1985. Fitting Fisher distributions to discontinuity orientation data. J. Geol. Educ. 33, 266–269. https://doi.org/10.5408/0022-1368-33.5.266.
Lato, M.J., Diederichs, M.S., Hutchinson, D.J., 2010. Bias correction for view-limited lidar scanning of rock outcrops for structural characterization. Rock Mech. Rock Eng. 43, 615–625. https://doi.org/10.1007/s00603-010-0086-5.
Lato, M.J., Diederichs, M.S., Hutchinson, D.J., Harrap, R., 2012. Evaluating roadside rockmasses for rockfall hazards using LiDAR data: optimizing data collection and processing protocols. Nat. Hazards 60, 831–864. https://doi.org/10.1007/s11069-011-9872-y.
Lato, M., Kemeny, J., Harrap, R.M., Bevan, G., 2013. Rock bench: establishing a common repository and standards for assessing rockmass characteristics using LiDAR and photogrammetry. Comput. Geosci. 50, 106–114. https://doi.org/10.1016/j.cageo.2012.06.014.
Lemy, F., Hadjigeorgiou, J., 2003. Discontinuity trace map construction using photographs of rock exposures. Int. J. Rock Mech. Min. Sci. 40, 903–917. https://doi.org/10.1016/S1365-1609(03)00069-8.
Leng, X., Xiao, J., Wang, Y., 2016. A multi-scale plane-detection method based on the Hough transform and region growing. Photogramm. Rec. 31, 166–192. https://doi.org/10.1111/phor.12145.
Li, X., Chen, J., Zhu, H., 2016. A new method for automated discontinuity trace mapping on rock mass 3D surface model. Comput. Geosci. 89, 118–131. https://doi.org/10.1016/j.cageo.2015.12.010.
Li, L., Yang, F., Zhu, H., Li, D., Li, Y., Tang, L., 2017. An improved RANSAC for 3D point cloud plane segmentation based on normal distribution transformation cells. Rem. Sens. 9 https://doi.org/10.3390/rs9050433.
Li, J., Yang, B., Cong, Y., Cao, L., Fu, X., Dong, Z., 2019. 3D forest mapping using a low-cost UAV laser scanning system: investigation and comparison. Rem. Sens. 11, 717. https://doi.org/10.3390/RS11060717.
Li, X., Chen, Z., Chen, J., Zhu, H., 2019. Automatic characterization of rock mass discontinuities using 3D point clouds. Eng. Geol. 259, 105131 https://doi.org/10.1016/j.enggeo.2019.05.008.
Limberger, F.A., Oliveira, M.M., 2015. Real-time detection of planar regions in unorganized point clouds. Pattern Recogn. 48, 2043–2053. https://doi.org/10.1016/j.patcog.2014.12.020.
Liu, L., Xiao, J., Wang, Y., 2019. Major orientation estimation-based rock surface extraction for 3D rock-mass point clouds. Rem. Sens. 11, 635. https://doi.org/10.3390/rs11060635.
Maalek, R., Lichti, D.D., Ruwanpura, J.Y., 2018. Robust segmentation of planar and linear features of terrestrial laser scanner point clouds acquired from construction sites. Sensors (Switzerland) 18, 819. https://doi.org/10.3390/s18030819.
Mallet, C., Bretar, F., Roux, M., Soergel, U., Heipke, C., 2011. Relevance assessment of full-waveform lidar data for urban area classification. ISPRS J. Photogrammetry Remote Sens. 66, S71. https://doi.org/10.1016/j.isprsjprs.2011.09.008. –S84.
Maquet, J.F., 2010. Construction Methods and Planning, eighth ed. Pearson Education, London, UK. https://doi.org/10.1139/l95-122.
Martinez, J.G., Albeaino, G., Gheisari, M., Volkmann, W., Alarcón, L.F., 2021. UAS point cloud accuracy assessment using structure from motion–based photogrammetry and PPK georeferencing technique for building surveying applications. J. Comput. Civ. Eng. 35, 05020004 https://doi.org/10.1061/(asce)cp.1943-5487.0000936.
Matas, J., Galambos, C., Kittler, J., 2000. Robust detection of lines using the progressive probabilistic hough transform. Comput. Vis. Image Understand. 78, 119–137. https://doi.org/10.1006/cviu.1999.0831.
Menegoni, N., Giordan, D., Perotti, C., Tannant, D.D., 2019. Detection and geometric characterization of rock mass discontinuities using a 3D high-resolution digital outcrop model generated from RPAS imagery – ormea rock slope. Italy. Eng. Geol. 252, 145–163. https://doi.org/10.1016/j.enggeo.2019.02.028.
Morsdorf, F., Meier, E., Kötz, B., Itten, K.I., Dobbertin, M., Allgöwer, B., 2004. LIDAR-based geometric reconstruction of boreal type forest stands at single tree level for forest and wildland fire management. In: Remote Sensing of Environment. Elsevier Inc., pp. 353–362. https://doi.org/10.1016/j.rse.2004.05.013
Nex, F., Remondino, F., 2014. UAV for 3D mapping applications: a review. Appl. Geomatics. https://doi.org/10.1007/s12518-013-0120-x.
Nguyen, A., Le, B., 2013. 3D point cloud segmentation: a survey. In: IEEE Conference on Robotics, Automation and Mechatronics, RAM - Proceedings. IEEE Computer Society, pp. 225–230. https://doi.org/10.1109/RAM.2013.6758588.
Nurunnabi, A., Belton, D., West, G., 2012. Robust segmentation in laser scanning 3D point cloud data. In: 2012 International Conference on Digital Image Computing Techniques and Applications. https://doi.org/10.1109/DICTA.2012.6411672. Dicta 2012.
Nurunnabi, A., Belton, D., West, G., 2014. Robust statistical approaches for local planar surface fitting in 3D laser scanning data. ISPRS J. Photogrammetry Remote Sens. 96, 106–122. https://doi.org/10.1016/j.isprsjprs.2014.07.004.
Nurunnabi, A., West, G., Belton, D., 2015. Outlier detection and robust normal-curvature estimation in mobile laser scanning 3D point cloud data. Pattern Recogn. 48, 1404–1419. https://doi.org/10.1016/j.patcog.2014.10.014.
O'Banion, M.S., Olsen, M.J., Rault, C., Wartman, J., Cunningham, K., 2018. Suitability of structure from motion for rock-slope assessment. Photogramm. Rec. 33, 217–242. https://doi.org/10.1111/phor.12241.
Pauly, M., Gross, M., Kobbelt, L.P., 2002. Efficient simplification of point-sampled surfaces. In: Proceedings of the IEEE Visualization Conference, pp. 163–170. https://doi.org/10.1109/visual.2002.1183771.
Pauly, M., Keiser, R., Gross, M., 2003. Multi-scale feature extraction on point-sampled surfaces. In: Computer Graphics Forum. Blackwell Publishing Ltd, pp. 281–289. https://doi.org/10.1111/1467-8659.00675.
Priest, S.D., Hudson, J.A., 1981. Estimation of discontinuity spacing and trace length using scanline surveys. Int. J. Rock Mech. Min. Sci. Geomech. Abstr. 18, 183–197. https://doi.org/10.1016/0148-9062(81)90973-6.
Pu, S., Vosselman, G., 2006. Automatic extraction of building features from terrestrial laser scanning. In: International Archives of Photogrammetry, pp. 25–27 https://doi.org/1011.222.2486.
Qi, C.R., Su, H., Mo, K., Guibas, L.J., 2017a. PointNet: deep learning on point sets for 3D classification and segmentation. In: Proceedings - 30th IEEE Conference on Computer Vision and Pattern Recognition, CVPR 2017. Institute of Electrical and Electronics Engineers Inc., pp. 77–85. https://doi.org/10.1109/CVPR.2017.16
Qi, C.R., Yi, L., Su, H., Guibas, L.J., 2017b. PointNet++: deep hierarchical feature learning on point sets in a metric space. In: Advances in Neural Information Processing Systems, pp. 5100–5109.
Qin, R., Tian, J., Reinartz, P., 2016. 3D change detection – approaches and applications. ISPRS J. Photogrammetry Remote Sens. https://doi.org/10.1016/j.isprsjprs.2016.09.013.
Rabbani, T., van den Wildenberg, F., Vosselman, G., 2006. Segmentation of point clouds using smoothness constraint. In: International Archives of Photogrammetry, Remote Sensing and Spatial Information Sciences, pp. 248–253.
Raguram, R., Frahm, J.M., Pollefeys, M., 2008. A comparative analysis of RANSAC techniques leading to adaptive real-time random sample consensus. Lect. Notes Comput. Sci. https://doi.org/10.1007/978-3-540-88688-4_37.
Raguram, R., Chum, O., Pollefeys, M., Matas, J., Frahm, J.M., 2013. USAC: a universal framework for random sample consensus. IEEE Trans. Pattern Anal. Mach. Intell. 35, 2022–2038. https://doi.org/10.1109/TPAMI.2012.257.
Rathje, E.M., Franke, K., 2016. Remote sensing for geotechnical earthquake reconnaissance. Soil Dynam. Earthq. Eng. 91, 304–316. https://doi.org/10.1016/j.soildyn.2016.09.016.
Reid, T.R., Harrison, J.P., 1997. Automated tracing of rock mass discontinuities from digital images. Int. J. Rock Mech. Min. Sci. 34, 256.e1–256.e19. https://doi.org/10.1016/S1365-1609(97)00281-5.
Riquelme, A.J., Abellán, A., Tomás, R., Jaboyedoff, M., 2014. A new approach for semi-automatic rock mass joints recognition from 3D point clouds. Comput. Geosci. 68, 38–52. https://doi.org/10.1016/j.cageo.2014.03.014.
Riquelme, A.J., Abellán, A., Tomás, R., 2015. Discontinuity spacing analysis in rock masses using 3D point clouds. Eng. Geol. 195, 185–195. https://doi.org/10.1016/j.enggeo.2015.06.009.
Rodriguez, A., Laio, A., 2014. Clustering by fast search and find of density peaks. Science 344, 1492–1496. https://doi.org/10.1126/science.1242072, 80-.
Rottensteiner, F., Trinder, J., Clode, S., Kubik, K., 2005. Using the Dempster-Shafer method for the fusion of LIDAR data and multi-spectral images for building detection. Inf. Fusion 6, 283–300. https://doi.org/10.1016/j.inffus.2004.06.004.
Rusu, R.B., Cousins, S., 2011. 3D is here: point cloud library (PCL). In: Proceedings - IEEE International Conference on Robotics and Automation. https://doi.org/10.1109/ICRA.2011.5980567.
Sampath, A., Shan, J., 2006. Clustering based planar roof extraction from lidar data. In: American Society for Photogrammetry and Remote Sensing - Annual Conference of the American Society for Photogrammetry and Remote Sensing 2006: Prospecting for Geospatial Information Integration, pp. 1262–1267.
Sampath, A., Shan, J., 2010. Segmentation and reconstruction of polyhedral building roofs from aerial lidar point clouds. IEEE Trans. Geosci. Rem. Sens. 48, 1554–1567. https://doi.org/10.1109/TGRS.2009.2030180.
Sankey, T., Donager, J., McVay, J., Sankey, J.B., 2017. UAV lidar and hyperspectral fusion for forest monitoring in the southwestern USA. Remote Sens. Environ. 195, 30–43. https://doi.org/10.1016/j.rse.2017.04.007.
Schnabel, R., Wahl, R., Klein, R., 2007. Efficient RANSAC for point-cloud shape detection. Comput. Graph. Forum 26, 214–226. https://doi.org/10.1111/j.1467-8659.2007.01016.x.
Seheult, A.H., Green, P.J., Rousseeuw, P.J., Leroy, A.M., 1989. Robust regression and outlier detection. J. R. Stat. Soc. Ser. A (Statistics Soc. 152, 133. https://doi.org/10.2307/2982847.
Shahzad, M., Zhu, X.X., Bamler, R., 2012. Façade structure reconstruction using spaceborne TomoSAR point clouds. In: International Geoscience and Remote Sensing Symposium (IGARSS), pp. 467–470. https://doi.org/10.1109/IGARSS.2012.6351385.
Sinaga, K.P., Yang, M.S., 2020. Unsupervised K-means clustering algorithm. IEEE Access 8, 80716–80727. https://doi.org/10.1109/ACCESS.2020.2988796.
Singh, S.K., Raval, S., Banerjee, B.P., 2021. Automated structural discontinuity mapping in a rock face occluded by vegetation using mobile laser scanning. Eng. Geol. 285, 106040 https://doi.org/10.1016/j.enggeo.2021.106040.
Slob, S., 2010. Automated Rock Mass Characterisation Using 3-D Terrestrial Laser Scanning. PhD thesis. Delft University of Technology (PhD thesis)., https://doi.org/0166077.
Smith, J.V., Holden, L., 2021. Rock slope kinematic instability controlled by large-scale variation of basalt column orientation. Bull. Eng. Geol. Environ. 80, 239–250. https://doi.org/10.1007/s10064-020-01917-5.
Snavely, N., Seitz, S.M., Szeliski, R., 2006. Photo tourism: exploring photo collections in 3D. In: ACM SIGGRAPH 2006 Papers, SIGGRAPH '06. ACM Press, New York, New York, USA, pp. 835–846. https://doi.org/10.1145/1179352.1141964.

Snavely, N., Seitz, S.M., Szeliski, R., 2008. Modeling the world from Internet photo collections. Int. J. Comput. Vis. 80, 189–210. https://doi.org/10.1007/s11263-007-0107-3.

Su, Y.T., Bethel, J., Hu, S., 2016. Octree-based segmentation for terrestrial LiDAR point cloud data in industrial applications. ISPRS J. Photogrammetry Remote Sens. 113, 59–74. https://doi.org/10.1016/j.isprsjprs.2016.01.001.

Tanimoto, C., Murai, S., Kiyama, H., Michihiro, K., 1991. Hydraulic behaviour of rock joints through the infrared photo image analysis. In: 7th ISRM Congress. International Society for Rock Mechanics and Rock Engineering, pp. 623–626. https://doi.org/10.1016/0148-9062(93)90409-7.

Tannant, D., 2015. Review of photogrammetry-based techniques for characterization and hazard assessment of rock faces. Int. J. Geohazards Environ 1, 76–87. https://doi.org/10.15273/ijge.2015.02.009.

Tarsha-Kurdi, F., Landes, T., Grussenmeyer, P., 2008a. Hough-Transform and extended RANSAC algorithms for automatic detection of 3D building roof Planes from Lidar data. In: ISPRS Workshops on Laser Scanning 2007 and SilviLaser 2007. Sep 2007, Espoo, Finland.

Tarsha-Kurdi, F., Landes, T., Grussenmeyer, P., 2008b. Extended ransac algorithm for automatic detection of building roof planes from lidar data. Photogramm. J. Finland 21, 97–109.

Torr, P.H.S., Zisserman, A., 2000. MLESAC: a new robust estimator with application to estimating image geometry. Comput. Vis. Image Understand. 78, 138–156. https://doi.org/10.1006/cviu.1999.0832.

Toshev, A., Mordohai, P., Taskar, B., 2010. Detecting and parsing architecture at city scale from range data. In: Proceedings of the IEEE Computer Society Conference on Computer Vision and Pattern Recognition, pp. 398–405. https://doi.org/10.1109/CVPR.2010.5540187.

Toth, C.K., 2009. R&D of mobile LiDAR mapping and future trends. In: American Society for Photogrammetry and Remote Sensing Annual Conference 2009. ASPRS, pp. 829–835, 2009.

Tovari, D., Pfeifer, N., 2005. Segmentation based robust interpolation – a new approach to laser data filtering. Laserscanning 2005 IAPRS 6.

Triggs, B., McLauchlan, P.F., Hartley, R.I., Fitzgibbon, A.W., 2000. Bundle adjustment – a modern synthesis. In: Lecture Notes in Computer Science (Including Subseries Lecture Notes in Artificial Intelligence and Lecture Notes in Bioinformatics). Springer Verlag, pp. 298–372. https://doi.org/10.1007/3-540-44480-7_21.

Vo, A.V., Truong-Hong, L., Laefer, D.F., Bertolotto, M., 2015. Octree-based region growing for point cloud segmentation. ISPRS J. Photogrammetry Remote Sens. 104, 88–100. https://doi.org/10.1016/j.isprsjprs.2015.01.011.

Vöge, M., Lato, M.J., Diederichs, M.S., 2013. Automated rockmass discontinuity mapping from 3-dimensional surface data. Eng. Geol. 164, 155–162. https://doi.org/10.1016/j.enggeo.2013.07.008.

Wang, Z., Zhang, L., Fang, T., Mathiopoulos, P.T., Tong, X., Qu, H., Xiao, Z., Li, F., Chen, D., 2015. A multiscale and hierarchical feature extraction method for terrestrial laser scanning point cloud classification. IEEE Trans. Geosci. Rem. Sens. 53, 2409–2425. https://doi.org/10.1109/TGRS.2014.2359951.

Wang, X., Zou, L., Shen, X., Ren, Y., Qin, Y., 2017. A region-growing approach for automatic outcrop fracture extraction from a three-dimensional point cloud. Comput. Geosci. 99, 100–106. https://doi.org/10.1016/j.cageo.2016.11.002.

Wang, Y., Sun, Y., Liu, Z., Sarma, S.E., Bronstein, M.M., Solomon, J.M., 2019. Dynamic graph Cnn for learning on point clouds. ACM Trans. Graph. 38 https://doi.org/10.1145/3326362.

Wehr, A., Lohr, U., 1999. Airborne laser scanning - an introduction and overview. ISPRS J. Photogrammetry Remote Sens. 54, 68–82. https://doi.org/10.1016/S0924-2716(99)00011-8.

Weinmann, M., Jutzi, B., Hinz, S., Mallet, C., 2015. Semantic point cloud interpretation based on optimal neighborhoods, relevant features and efficient classifiers. ISPRS J. Photogrammetry Remote Sens. 105, 286–304. https://doi.org/10.1016/j.isprsjprs.2015.01.016.

West, K.F., Webb, B.N., Lersch, J.R., Pothier, S., Triscari, J.M., Iverson, A.E., 2004. Context-driven automated target detection in 3D data. In: Sadjadi, F.A. (Ed.), Automatic Target Recognition XIV. SPIE, pp. 133–143. https://doi.org/10.1117/12.542536.

Westoby, M.J., Brasington, J., Glasser, N.F., Hambrey, M.J., Reynolds, J.M., 2012. Structure-from-Motion" photogrammetry: a low-cost, effective tool for geoscience applications. Geomorphology 179, 300–314. https://doi.org/10.1016/j.geomorph.2012.08.021.

Wolff, K., Kim, C., Zimmer, H., Schroers, C., Botsch, M., Sorkine-Hornung, O., Sorkine-Hornung, A., 2016. Point cloud noise and outlier removal for image-based 3D reconstruction. In: Proceedings - 2016 4th International Conference on 3D Vision, 3DV. Institute of Electrical and Electronics Engineers Inc., pp. 118–127. https://doi.org/10.1109/3DV.2016.20, 2016.

Xiao, J., Zhang, Jianhua, Adler, B., Zhang, H., Zhang, Jianwei, 2013. Three-dimensional point cloud plane segmentation in both structured and unstructured environments. Robot. Autonom. Syst. 61, 1641–1652. https://doi.org/10.1016/j.robot.2013.07.001.

Xie, Y., Tian, J., Zhu, X.X., 2020. Linking points with labels in 3D: a review of point cloud semantic segmentation. IEEE Geosci. Remote Sens. Mag. https://doi.org/10.1109/MGRS.2019.2937630.

Ximin, Z., Wanggen, W., Li, X., Junxing, M., 2015. Mean shift clustering segmentation and RANSAC simplification of color point cloud. In: ICALIP 2014 - 2014 International Conference on Audio, Language and Image Processing, Proceedings. Institute of Electrical and Electronics Engineers Inc., pp. 837–841. https://doi.org/10.1109/ICALIP.2014.7009912

Xu, D., Tian, Y., 2015. A comprehensive survey of clustering algorithms. Ann. Data Sci. 2, 165–193. https://doi.org/10.1007/s40745-015-0040-1.

Xu, L., Oja, E., Kultanen, P., 1990. A new curve detection method: Randomized Hough transform (RHT). Pattern Recogn. Lett. 11, 331–338. https://doi.org/10.1016/0167-8655(90)90042-Z.

Xu, B., Jiang, W., Shan, J., Zhang, J., Li, L., 2016. Investigation on the weighted RANSAC approaches for building roof plane segmentation from LiDAR point clouds. Rem. Sens. 8 https://doi.org/10.3390/rs8010005.

Xu, Y., Yao, W., Tuttas, S., Hoegner, L., Stilla, U., 2018. Unsupervised segmentation of point clouds from buildings using hierarchical clustering based on Gestalt principles. IEEE J. Sel. Top. Appl. Earth Obs. Rem. Sens. 11, 4270–4286. https://doi.org/10.1109/JSTARS.2018.2817227.

Yan, W.Y., Shaker, A., El-Ashmawy, N., 2015. Urban land cover classification using airborne LiDAR data: a review. Remote Sens. Environ. 158, 295–310. https://doi.org/10.1016/j.rse.2014.11.001.

YlaJaaski, A., Kiryati, N., 1994. Adaptive termination of voting in the probabilistic circular Hough transform. IEEE Trans. Pattern Anal. Mach. Intell. 16, 911–915. https://doi.org/10.1109/34.310688.

Yu, D., Xiao, J., Wang, Y., 2020. High-precision plane detection method for rock-mass point clouds based on supervoxel. Sensors (Switzerland) 20, 1–22. https://doi.org/10.3390/s20154209.

Zhang, P., Du, K., Tannant, D.D., Zhu, H., Zheng, W., 2018. Automated method for extracting and analysing the rock discontinuities from point clouds based on digital surface model of rock mass. Eng. Geol. 239, 109–118. https://doi.org/10.1016/J.ENGGEO.2018.03.020.

Zhang, P., Zhao, Q., Tannant, D.D., Ji, T., Zhu, H., 2019. 3D mapping of discontinuity traces using fusion of point cloud and image data. Bull. Eng. Geol. Environ. 78, 2789–2801. https://doi.org/10.1007/s10064-018-1280-z.

Zhang, X., Gao, R., Sun, Q., Cheng, J., 2019. An automated rectification method for unmanned aerial vehicle LiDAR point cloud data based on laser intensity. Rem. Sens. 11, 811. https://doi.org/10.3390/rs11070811.

Zhu, X.X., Shahzad, M., 2014. Facade reconstruction using multiview spaceborne TomoSAR point clouds. IEEE Trans. Geosci. Rem. Sens. 52, 3541–3552. https://doi.org/10.1109/TGRS.2013.2273619.

Zhu, Y., Ting, K.M., Carman, M.J., 2016. Density-ratio based clustering for discovering clusters with varying densities. Pattern Recogn. 60, 983–997. https://doi.org/10.1016/j.patcog.2016.07.007.

CloudCompare User Manual. https://www.cloudcompare.org. (Accessed 11 January 2021).

Point Cloud Library (PCL). http://pointclouds.org/documentation/. (Accessed 17 March 2022).

ShapeMetrix 3D. https://3gsm.at/produkte/shape-metrix/ (Accessed 05 January 2022).

Split-FX Analysis Service. https://www.maptek.com/products/pointstudio. (Accessed 11 August 2021).